NACA RM L56B21

NACA

RESEARCH MEMORANDUM

WIND-TUNNEL INVESTIGATION OF A RAM-JET MISSILE MODEL HAVING A WING AND CANARD SURFACES OF DELTA PLAN FORM WITH 70° SWEPT LEADING EDGES

FORCE AND MOMENT CHARACTERISTICS AT COMBINED ANGLES OF PITCH AND SIDESLIP FOR MACH NUMBER 2.01

By Cornelius Driver and Clyde V. Hamilton

Langley Aeronautical Laboratory
Langley Field, Va.

NATIONAL ADVISORY COMMITTEE FOR AERONAUTICS

WASHINGTON

April 26, 1956
Declassified January 20, 1958

NACA RM L56B21

NATIONAL ADVISORY COMMITTEE FOR AERONAUTICS

RESEARCH MEMORANDUM

WIND-TUNNEL INVESTIGATION OF A RAM-JET MISSILE MODEL HAVING A WING AND CANARD SURFACES OF DELTA PLAN FORM WITH 70° SWEPT LEADING EDGES

FORCE AND MOMENT CHARACTERISTICS AT COMBINED ANGLES OF PITCH AND SIDESLIP FOR MACH NUMBER 2.01

By Cornelius Driver and Clyde V. Hamilton

SUMMARY

An investigation has been conducted in the Langley 4- by 4-foot supersonic pressure tunnel to determine the static stability and control characteristics of a ram-jet canard missile at a Mach number of 2.01. The missile had wings and canard surfaces of delta plan form with 70° swept leading edges. Two ram-jet nacelles were mounted in the vertical plane on unswept pylons near the rear of the body. The center of gravity of the model was at -19.5 percent of the wing mean aerodynamic chord. Force characteristics of the missile configuration and various combinations of its components were determined through an incidence angle range from -2° to about 26° and at various roll angles from 0° to -90°. The Reynolds number of the investigation was 3.47×10^6 based on the wing mean aerodynamic chord.

An analysis of the results indicated that the missile became unstable in pitch above a lift coefficient of about 0.4 as a result, primarily, of the large unstable moment of the body.

The maximum lift-drag ratio was reduced from 5.0 to 3.2 by the addition of the nacelle-pylon combination to the wing-body-canard configuration.

There was a decrease in the directional stability at small angles of sideslip with increasing angle of attack up to angles of attack near 14°.

For positive angles of attack, the missile had negative effective dihedral or positive rolling moment due to sideslip.

INTRODUCTION

Tests have been made in the Langley 4- by 4-foot supersonic pressure tunnel to determine the aerodynamic characteristics of a ram-jet canard-missile configuration. The tests were part of a coordinated program with the Pilotless Aircraft Research Division to provide preflight aerodynamic characteristics of a model of a missile to be flight tested. In addition, tests were required to determine certain interference effects not obtainable in flight.

The model had a wing and horizontal and vertical canard surfaces of delta plan form with 70° swept leading edges. Two ram-jet nacelles were mounted in the vertical plane on short unswept pylons near the rear of the body. The model was equipped with all-movable canard control surfaces for both pitch and sideslip control, and movable wing-tip ailerons for roll control. The various component parts of the model could be removed to permit the investigation of the complete configuration or various combinations of its component parts to determine interference effects. The results of previous tests of the missile at a Mach number of 1.6 are presented in references 1 and 2.

The present paper presents the results of an extension to the investigation in which the static stability and control characteristics of the complete configuration and various combinations of its component parts were determined at a Mach number of 2.01 and a Reynolds number of of 3.47×10^6 based on the wing mean aerodynamic chord.

SYMBOLS

The results of the tests are presented as standard NACA coefficients of forces and moments. The data are referred to the stability-axis system (fig. 1) with the reference center of gravity at -19.5 percent of the wing mean aerodynamic chord.

b wing span, 0.988 ft

c wing section chord

$\bar{c}$ wing mean aerodynamic chord, $\frac{2}{S}\int_0^{b/2} c^2 dy$, 0.957 ft

D drag, lb

F	body frontal area, 0.03875 sq ft
l	body length, 4.23 ft
L	lift, lb
M_X	moment about X-axis, lb ft
M	Mach number
M_Y	moment about Y-axis, lb ft
M_Z	moment about Z-axis, lb ft
q	free-stream dynamic pressure, lb/sq ft
S	total wing area, 0.6948 sq ft (see fig. 2)
x	longitudinal distance from mean geometric chord
y	distance along wing span from model center line measured normal to the plane of symmetry
X	force along X-axis, lb
Y	force along Y-axis, lb
Z	force along Z-axis, lb
C_L	lift coefficient, Lift/qS (where lift is -Z)
C_X	longitudinal-force coefficient, X/qS ($-C_X = C_D$ when $\beta = 0$)
C_m	pitching-moment coefficient, $M'/qS\bar{c}$
C_Y	lateral-force coefficient, Y/qS
C_l	rolling-moment coefficient, L/qSb
C_n	yawing-moment coefficient, N/qSb
α	angle of attack of the body center line, deg
β	angle of sideslip of the body center line, deg

i incidence angle, deg (angle between body center line and relative wind or sting angle)

ϕ angle of roll about the body axis, deg (positive angles clockwise as viewed from rear). ϕ is zero when the wings are in a plane 90° from the plane containing the incidence angle i

δ_V vertical canard deflection, deg

δ_H horizontal canard deflection, deg

δ_{a_R} aileron deflection, right, deg

δ_{a_L} aileron deflection, left, deg

Notation for configuration:

B body

W wing

C horizontal and vertical canard surfaces

N nacelles

MODEL AND APPARATUS

A three-view drawing of the basic model is shown in figure 2(a). Details of the canard surfaces and the method of determining wing area included within the body are presented in figure 2(b). A photograph showing the details of the model is shown in figure 3. The geometric characteristics of the model are given in table I.

The model was composed of a cylindrical body with a nose formed by a parabolic section and a frustum of a cone. Coordinates for the body are given in table II. The canard surfaces were in both the horizontal and vertical planes and had delta plan forms with 70° swept leading edges. The canard surfaces were all-moving and were deflected about axes normal to the body center line.

The main wing was located in the horizontal plane and had a modified delta plan form with 70° swept leading edges. (See fig. 2(c).) The nacelles were mounted on short, unswept pylons near the rear of the

body and correspond to the position designated "aft inboard" in reference 1. Coordinates for the nacelle and nacelle center body are given in Table III. All components of the model were removable so that tests of various combinations of components could be made.

The model was mounted on a remotely controlled rotary-type sting so that tests could be made at various roll angles of the model. Force measurements were obtained through the use of a six-component internal strain-gage balance.

TESTS AND PROCEDURE

Tests were made through a sting angle range from -2° to about 26° at various roll angles from 0° to -90°. The sting angles and roll angles were resolved into the angles of attack α and sideslip β by means of the following relations:

$$\tan \alpha = \tan i \cos \phi \qquad (1)$$

$$\tan \beta = \sin i \sin \phi \qquad (2)$$

The test conditions were

Mach number	2.01
Reynolds number, based on wing mean aerodynamic chord	3.47×10^6
Stagnation pressure, atm	1.0
Stagnation temperature, °F	100
Dewpoint, °F	below -25°

The model configurations tested are listed in the following table:

Incidence angle i, deg	Roll angle, φ, deg	Model configuration	Horizontal canard deflection, δ_H, deg	Vertical canard deflection, δ_V, deg	Aileron deflection δ_a, deg
-2 to 27	0 to -90	Complete model (BWNC)	0, -8, -12	0, -10	0, ±10
-2 to 21	0, -45, -90	Body (B)	----------	------	------
0 to 26	0 to -90	Body-wing (BW)	----------	------	0
-2 to 12	0 to -90	Body-canards (BC)	0, -8, -12	0	------
-2 to 27	0 to -90	Body-wing-canards (BWC)	0	0	0
-2 to 27	0 to -90	Body-wing-canards - lower nacelle	0	0	0
-2 to 27	0 to -90	Body-wing-canards - upper nacelle	0	0	0

For all the test runs the nacelles were open and the data include the effects of internal flow. The nacelles were designed for a Mach number of 2 and, for this test, were operated near their design mass-flow ratio of 1.0. (For one run a pressure-survey rake was installed at the base of one nacelle and the mass-flow ratio was determined to be about 0.97.)

CORRECTIONS AND ACCURACY

A limited calibration prior to these tests has shown that the flow in the test section is reasonably uniform. The Mach number variation in the test sections was ±0.015 and the flow-angle variation in the horizontal and vertical planes was ±0.1°. No corrections were applied to the data to account for these flow variations. The angles of incidence were corrected for deflection under load. No corrections were applied to the roll angles due to deflection under load; however, these deflections would be small due to the comparatively small rolling moments and the rigidity of the system.

The base pressure was measured and the drag data were corrected to a base pressure equal to the free-stream static pressure. Errors in the base pressure measurements are included in the estimated error of C_X. No corrections were made for sting interference.

The estimated errors in the individual measured quantities are as follows:

C_m	±0.0004
C_N	±0.004
C_X	±0.002
C_n	±0.0005
C_l	±0.0004
C_Y	±0.001
i, deg	±0.1
φ, deg	±0.1
δ_H, deg	±0.1
δ_α, deg	±0.1

RESULTS

The basic results presented as functions of the incidence angle i for various constant values of roll angle φ are shown in the following manner:

Configuration	Figure
BWCN, $\delta_H = 0$	4
BWCN, $\delta_H = -8^\circ$	5
BWCN, $\delta_H = -12^\circ$	6
BWCN, $\delta_V = -10^\circ$	7
BWCN, $\delta_{a_L} = 10^\circ$, $\delta_{a_R} = -10^\circ$	8
BC, $\delta_H = 0^\circ$	9
BC, $\delta_H = -8^\circ$	10
BC, $\delta_H = -12^\circ$	11
BW	12
BWC, $\delta_H = 0$	13

Analysis figures obtained from the basic data are presented as follows:

Aerodynamic characteristics in pitch for several constant control deflections; $\beta = 0^\circ$	14
Effect of center-of-gravity location on the aerodynamic characteristics in pitch; $\beta = 0^\circ$	15
Aerodynamic characteristics in pitch of the complete model and various combinations of its components; $\beta = 0^\circ$	16
L/D ratios for the complete model and various combinations of its components; $\beta = 0^\circ$	17
Effect of nacelle location on the aerodynamic characteristics in pitch; $\beta = 0^\circ$	18
Aerodynamic characteristics in sideslip at vertical canard deflections of 0° and -10°; $\alpha = 0^\circ$	19
Aerodynamic characteristics in sideslip for the complete model and various combinations of its components; $\alpha = 0^\circ$	20
Effect of nacelle location on the aerodynamic characteristics in sideslip; $\alpha = 0^\circ$	21
Effect of vertical canard deflection on the aerodynamic characteristics in pitch; $\beta = 0^\circ$	22
Effect of horizontal canard deflection on the aerodynamic characteristics in sideslip; $\alpha = 0^\circ$	23
Effect of aileron deflection on the aerodynamic characteristics in pitch; $\beta = 0^\circ$	24
Effect of angle of attack on the aerodynamic characteristics in sideslip	25

Longitudinal Characteristics

Stability and control, complete model.- The pitching-moment curves for the complete model (fig. 14) indicate a large nonlinear moment variation with lift coefficient. Such nonlinear characteristics may lead to missile tumbling at higher angles of attack and may necessitate a restriction of the angle-of-attack range to angles below 12°. The results obtained at $M = 1.6$ (ref. 1) indicated a similar trend although the angle-of-attack range did not extend beyond 14°. A forward shift in center-of-gravity location of $-0.30\ x/\bar{c}$ eliminated the unstable variation of pitching-moment coefficient at high angles of attack (fig. 15) but also increased the static stability $-C_m/C_L$ to such an extent that the maneuverability could be seriously hampered.

At a center-of-gravity location of -19.5 percent of wing mean aerodynamic chord, the maximum trim lift coefficient in the stable range $\delta_H = -12°$, was approximately 0.4 at $\alpha = 12°$ and the resulting longitudinal-force coefficient was -0.14.

Effects of component parts.- The longitudinal characteristics of the complete model and various combinations of its components are presented in figure 16. The nonlinear pitching moment appears to be primarily a body effect rather than a wake or upwash effect (fig. 16) since the model with the canards removed indicates the same nonlinear trends. The addition of the nacelle-pylon combination to the body-wing canard configuration caused a large increase in minimum drag (fig. 16) and lowered the maximum L/D from 5.0 to 3.2 (fig. 17). The addition of the upper nacelle only (fig. 18) produced a positive moment increment which resulted from the combined effects of the drag of the nacelle-strut combination and the interference lift loss on the upper surface of the wing. Conversely, the combined interference and drag effects of the lower nacelle resulted in a negative moment increment. The addition of both nacelles produced a greater destabilizing effect on the complete configuration (fig. 18) than indicated by the results for the nacelles individually.

Lateral Characteristics

Directional stability and control, complete model.- The results for the complete configuration (fig. 19) indicate that the model is directionally stable up to sideslip angles near 14°. The pylons and nacelles provide greater lateral force and directional stability (fig. 20) than the wings provide normal force and longitudinal stability (fig. 16). As a result, potentially higher angles could be reached in the yaw plane before instability occurred. However, because of the greater stability and the decreased canard area, the vertical canard is less effective in producing trim angle changes than is the horizontal canard.

Effects of component parts.- The lateral characteristics of the complete model and various combinations of its components are presented in figures 20 and 21. The differences in side force and yawing moment at the higher angles of attack between the configurations with only an upper or lower nacelle (fig. 21) are believed to result from small asymmetries inherent in the model and model support system. The directional stability for the complete model is somewhat less than that indicated by a summation of the individual nacelles as a result, probably, of a mutual interference of the nacelles on the body sidewash.

Induced effects of canard controls.- The induced effects caused by vertical and horizontal canard deflections on the aerodynamic characteristics in pitch and sideslip are presented in figures 22 and 23. The variation with angle of attack of the aerodynamic characteristics resulting from control deflection (figs. 22 and 23) are similar to those shown for other types of canard missiles (ref. 3, for example) and may lead to complicated flight control problems for such missiles. It should be pointed out, however, that the induced effects, for the most part, occur at angles of attack that are greater than those that would be reached before longitudinal instability occurred.

Lateral control.- The effects on the aerodynamic characteristics in pitch of deflecting the ailerons $\pm 10^\circ$ are shown in figure 24. There are small decreases in lift and pitching moment and a slight increase in longitudinal force. The ailerons provide a constant roll increment throughout the angle-of-attack range but are relatively ineffective in producing roll. It is indicated that a $\pm 10^\circ$ deflection would be required to overcome the induced roll produced by the vertical canard at an angle of attack of 12° (for example, fig. 22).

Effect of angle of attack on aerodynamic characteristics in sideslip.- Through the use of the equations for α and β given under "Tests and Procedure," it is possible to obtain sideslip data at various constant angles of attack. This procedure has been followed and, as an example, the results for the complete model have been obtained from the basic data (figs. 4 and 7) for various constant angles of attack through the sideslip range. The tabulated results are presented in table IV, and the variation of the coefficients with sideslip for various constant angles of attack is shown in figure 25. These results indicate a decrease in the directional stability at small sideslip angles with increasing angles of attack up to about 14° (fig. 25). With increasing positive angles of attack the variation of rolling moment with sideslip indicates a negative effective dihedral $\left(\text{positive } C_{l_\beta}, \text{ fig. 25(a)}\right)$.

Similar figures showing the variations of the various coefficients for combined angles of α and β can be made for each model configuration for which results were obtained through the roll-angle range.

CONCLUSIONS

A ram-jet canard missile model having a wing and horizontal and vertical canard surfaces of delta plan form with 70° swept leading edges was tested in the Langley 4- by 4-foot supersonic pressure tunnel. The center of gravity of the model was at -19.5 percent of the mean aerodynamic chord. The force characteristics of the model and various combinations of its components were determined at a Mach number of 2.01 and a Reynolds number of 3.47×10^6 based on the wing mean aerodynamic chord. A summary of the results of investigation indicated the following conclusions:

1. A nonlinear pitching-moment variation with lift for the complete model that is probably caused by the moment variation of the body alone may result in missile tumbling above a lift coefficient of 0.4. A forward shift in the center-of-gravity location would alleviate the tumbling but would result in lower maneuverability.

2. The maximum lift-drag ratio obtained for the complete model was 3.2. The removal of the nacelle-pylon combination increased the lift-drag ratio to 5.0.

3. The directional stability at small sideslip angles of the complete model decreased as the angle of attack was increased to angles of attack near 14°.

4. For positive angles of attack, the complete model had negative effective dihedral.

Langley Aeronautical Laboratory,
National Advisory Committee for Aeronautics,
Langley Field, Va., February 10, 1956.

REFERENCES

1. Hamilton, Clyde V., Driver, Cornelius, and Sevier, John R., Jr.: Wind-Tunnel Investigation of a Ram-Jet Missile Model Having a Wing and Canard Surfaces of Delta Plan Form With 70° Swept Leading Edges. Force and Moment Characteristics of Various Combinations of Components at a Mach Number of 1.6. NACA RM L53A14, 1953.

2. Spearman, M. Leroy, and Robinson, Ross B.: Wind-tunnel Investigation of a Ram-Jet Missile Model Having a Wing and Canard surfaces of Delta Plan Form With 70° Swept Leading Edges. Longitudinal and Lateral Stability and Control Characteristics at a Mach Number of 1.60. NACA RM L52E15, 1952.

3. Spearman, M. Leroy: Effect of Large Deflections of a Canard Control and Deflections of a Wing-Tip Control on the Static-Stability and Induced-Roll Characteristics of a Cruciform Canard Missile at a Mach Number of 2.01. NACA RM L53K03, 1953.

TABLE I

GEOMETRIC CHARACTERISTICS OF MODEL

Body:	
Maximum diameter, in.	2.666
Length, in.	50.833
Fineness ratio	19.067
Base area, sq in.	5.583
Wing:	
Span, in.	11.853
Chord at body-wing intersection, in.	17.069
Chord at aileron break line, in.	4.606
Area (including that within body), sq in.	100.05
Aspect ratio	1.342
Sweep angle of leading edge, deg	70
Thickness ratio at body center line	0.0147
Thickness ratio at aileron break line	0.0543
Leading-edge half angle normal to leading edge, deg	7.8
Trailing-edge half angle, normal to trailing edge, deg	7.8
Mean aerodynamic chord, in.	11.48
Aileron:	
Area, sq in.	3.201
Mean aerodynamic chord, in.	3.071
Horizontal canard surfaces:	
Area (exposed), sq in.	6.406
Mean aerodynamic chord, in.	2.576
Vertical canard surfaces:	
Area (exposed), sq in.	3.203
Mean aerodynamic chord, in.	1.821

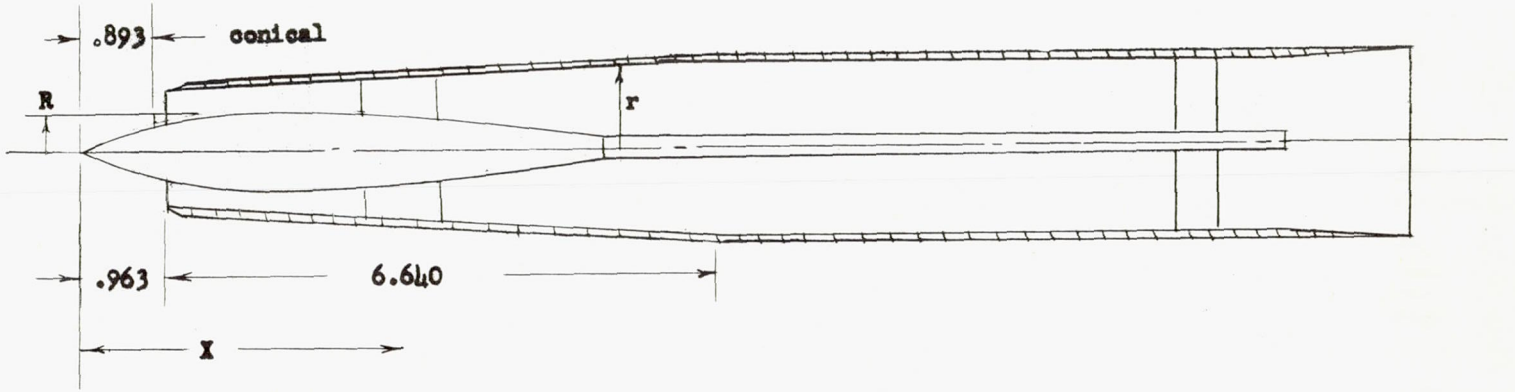
TABLE II

BODY COORDINATES

Body station	Radius	
0	0	
.297	.076	
.627	.156	
.956	.233	
1.285	.307	
1.615	.378	
1.945	.445	
2.275	.509	
2.605	.573	
2.936	.627	
3.267	.682	
3.598	.732	
3.929	.780	
4.260	.824	
4.592	.865	
4.923	.903	
5.255	.940	
5.587	.968	
5.920	.996	
6.252	1.020	
6.583	1.042	conical section
11.542	1.333	conical section
50.833	1.333	cylindrical section

TABLE III

NACELLE AND NACELLE-CENTER-BODY GEOMETRY



X	R	X	r
0	0	0.963	[a]0.706
.893	.325	7.603	[a].996
1.000	.360	13.712	[a].996
1.167	.402	14.962	[a]1.069
1.333	.429		
1.375	.433		
1.500	.441		
1.667	.443		
2.333	.418		
3.000	.375		
6.208	.157		

[a]All internal contours are straight between the points noted.

TABLE IV

TABULATED RESULTS FOR VARIOUS ANGLES OF ATTACK

AND SIDESLIP, COMPLETE MODEL

(a) $\delta_H = \delta_V = 0^\circ$

α, deg	ϕ, deg	i, deg	β, deg	C_n	C_l	C_Y	C_L	C_X	C_m
4	-15	4.14	-1.07	-0.005	-0.0001	0.023	0.125	-0.052	-0.0199
4	-25	4.41	-1.87	-.010	-.0001	.046	.130	-.053	-.0190
4	-35	4.88	-2.81	-.019	-.0001	.083	.131	-.053	-.0170
4	-45	5.65	-4.00	-.027	-.001	.130	.130	-.052	-.0100
4	-60	7.96	-6.91	-.053	-.005	.250	.125	-.052	-.0065
4	-70	11.56	-10.88	-.10	-.008	.435	.130		-.0100
4	-77	17.27	-16.85						
4	-80	21.94	-21.64						
8	-15	8.28	-2.16	-.0085	-.0001	.050	.260	-.081	-.037
8	-25	8.82	-3.75	-.020	-.002	.111	.265	-.081	-.038
8	-35	9.74	-5.62	-.041	-.01	.187	.270	-.081	-.034
8	-45	11.24	-8.00	-.068	-.014	.30	.260	-.081	-.032
8	-60	15.70	-13.68	-.122	-.019	.580	.280	-.083	-.026
8	-70	22.34	-21.11						
12	-15	12.01	-3.26	-.014	-.009	.085	.385	-.123	-.039
12	-25	13.20	-5.66	-.0396	-.019	.190	.40	-.130	-.041
12	-35	14.55	-8.46	-.069	-.028	.330	.415	-.132	-.041
12	-45	16.73	-12.00	-.115	-.032	.51	.425	-.133	-.039
12	-60	23.03	-20.21						
16	-15	16.54	-4.39	-.029	-.021	.135	.535	-.195	-.009
16	-25	17.56	-7.62	-.057	-.034	.30	.55	-.201	-.017
16	-35	19.29	-11.35	-.086	-.044	.495	.565	-.206	-.030
16	-45	22.07	-16.00		-.041				
20	-15	20.65	-5.57	-.074	-.034	.265	.685	-.298	.037
20	-25	21.88	-9.63	-.091	-.046	.45	.70	-.300	.023
20	-35	23.96	-14.30	-.180	-.056	.65	.70	-.306	.008
24	-15	24.75	-6.80	-.092	-.041	.35	.872		.030
24	-25	26.16	-11.73	-.097	-.055	.565	.880		.0001

TABLE IV.- Concluded

TABULATED RESULTS FOR VARIOUS ANGLES OF ATTACK

AND SIDESLIP, COMPLETE MODEL

(b) $\delta_H = 0^\circ$; $\delta_V = -10^\circ$

α, deg	ϕ, deg	i, deg	β, deg	C_L	C_X	C_m	C_l	C_n	C_Y
4	-15	4.14	-1.07	0.135	-0.057	-0.020	-0.001	0.048	0.012
4	-25	4.41	-1.87						
4	-35	4.88	-2.81	.131	-.051	-.017	-.003	.036	.093
4	-45	5.65	-4.00	.128	-.056	-.015	-.006	.021	.142
4	-60	7.96	-6.91	.115	-.059		-.008	-.010	.265
4	-70	11.56	-10.88						
4	-77	17.27	-16.85						
4	-80	21.94	-21.64						
8	-15	8.28	-2.16	.257	-.086	-.035	-.003	.039	.080
8	-25	8.82	-3.75						
8	-35	9.74	-5.62	.232	-.061	-.030	-.011	.003	.220
8	-45	11.24	-8.00	.255	-.087	-.034	-.016	-.024	.330
8	-60	15.70	-13.68	.267	-.096		-.015	-.091	.588
8	-70	22.34	-21.11						
12	-15	12.01	-3.26	.379	-.126	-.032	-.002	.018	.152
12	-25	13.20	-5.66						
12	-35	14.55	-8.46	.398	-.077	-.034	-.019	-.034	.370
12	-45	16.73	-12.00	.414		-.033	-.004	-.070	.530
12	-60	23.03	-20.21						
16	-15	16.54	-4.39	.543	-.200	-.009	-.001	-.017	.227
16	-25	17.56	-7.62						
16	-35	19.29	-11.35	.559	-.100	-.038	-.027	-.058	.515
16	-45	22.07	-16.00						
20	-15	20.65	-5.57	.712	-.307	-.001	-.010		.242
20	-25	21.88	-9.63						
20	-35	23.96	-14.30	.725	-.133	-.022	-.039	-.072	.658
24	-15	24.75	-6.80	.890	-.447	.023	-.023		.357
24	-25	26.16	-11.73						

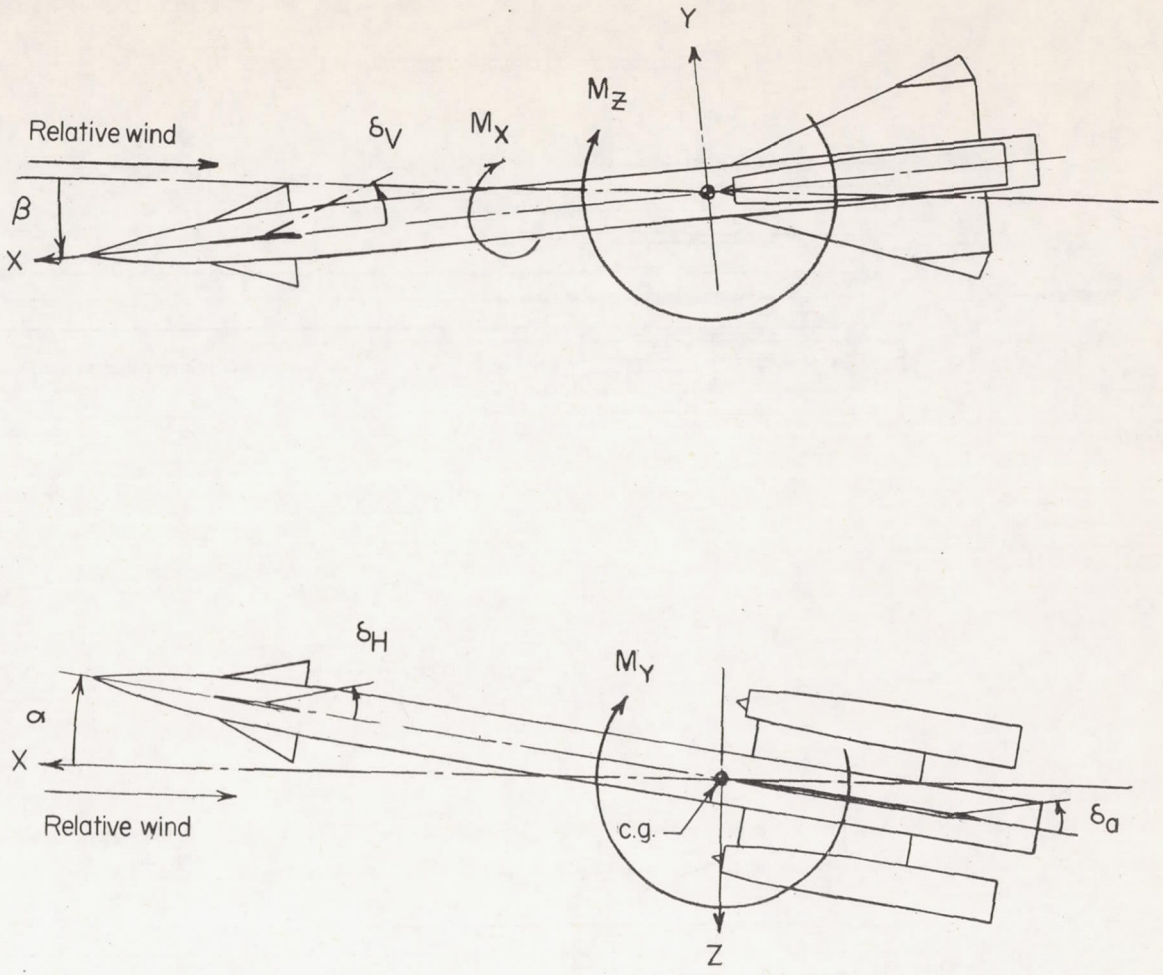
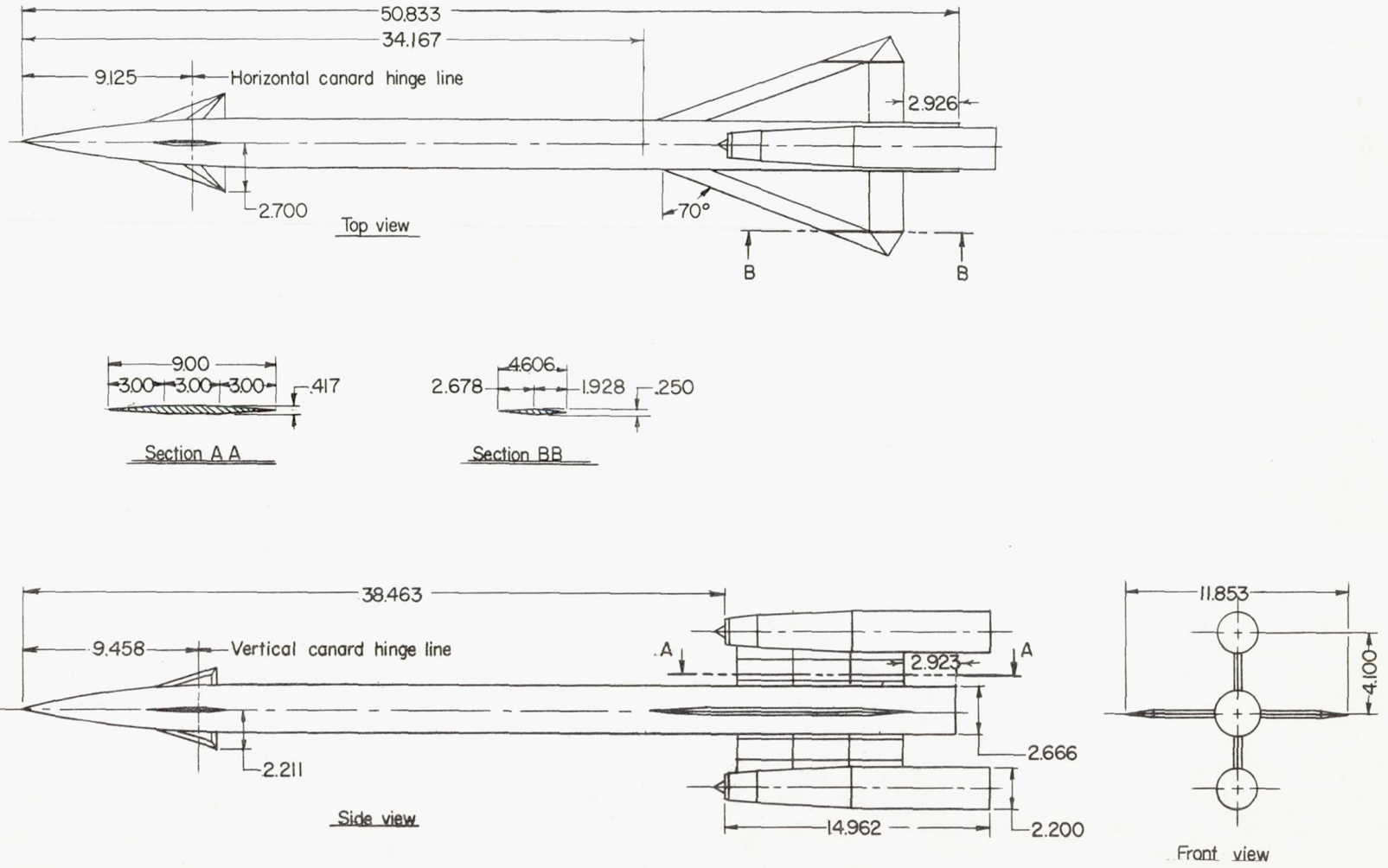
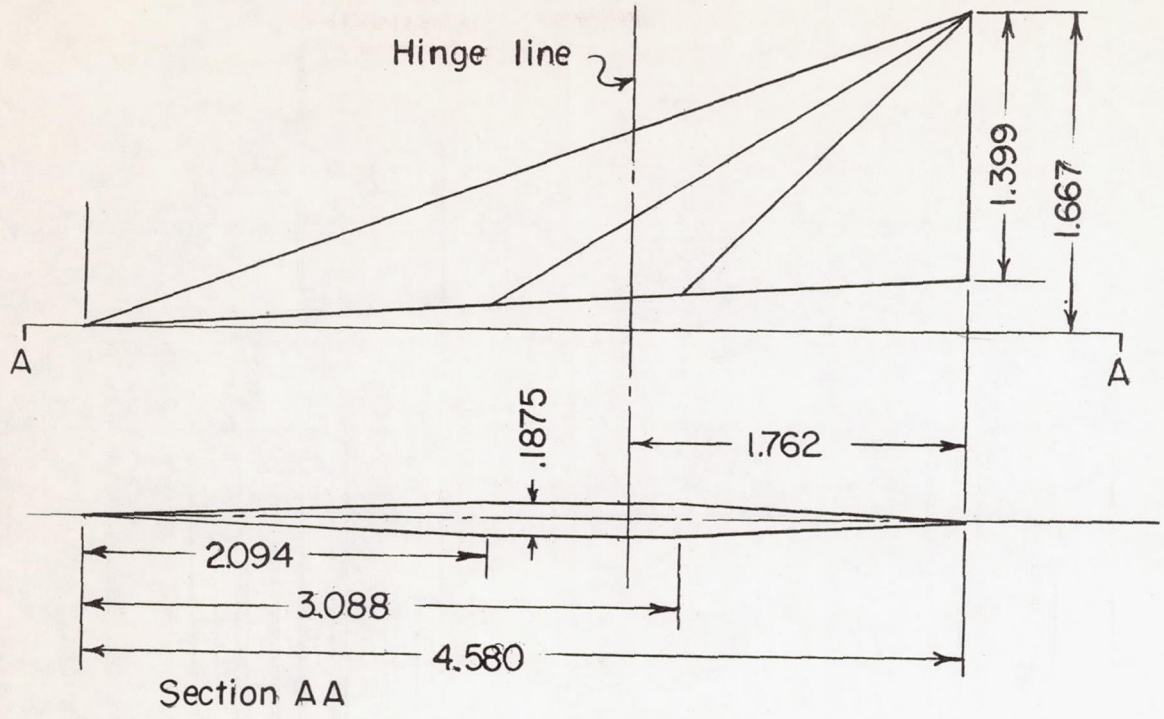


Figure 1.- System of stability axes. Arrows indicate positive values.

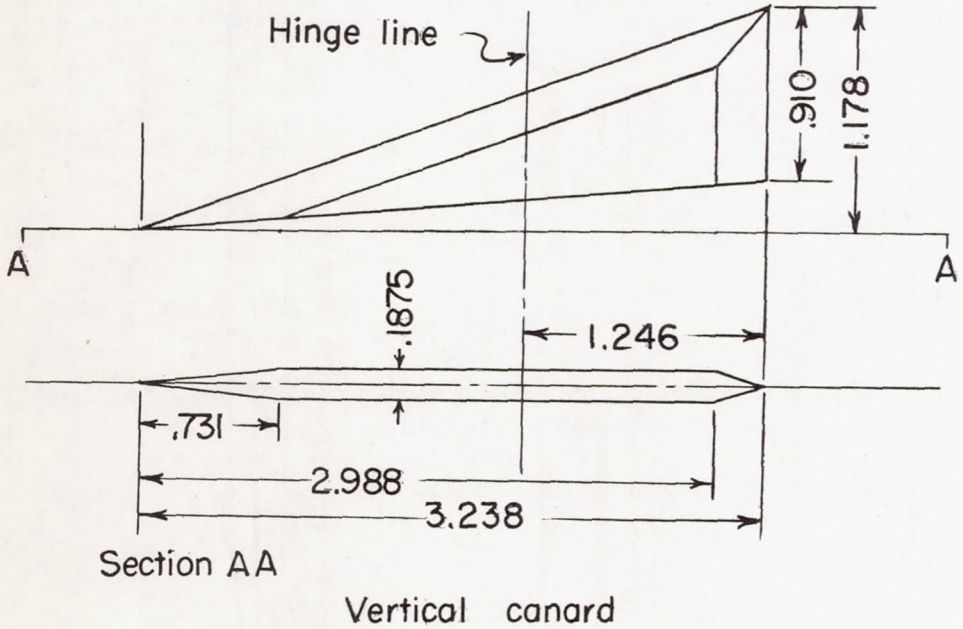


(a) General arrangement of model.

Figure 2.- Details of model. All dimensions in inches.



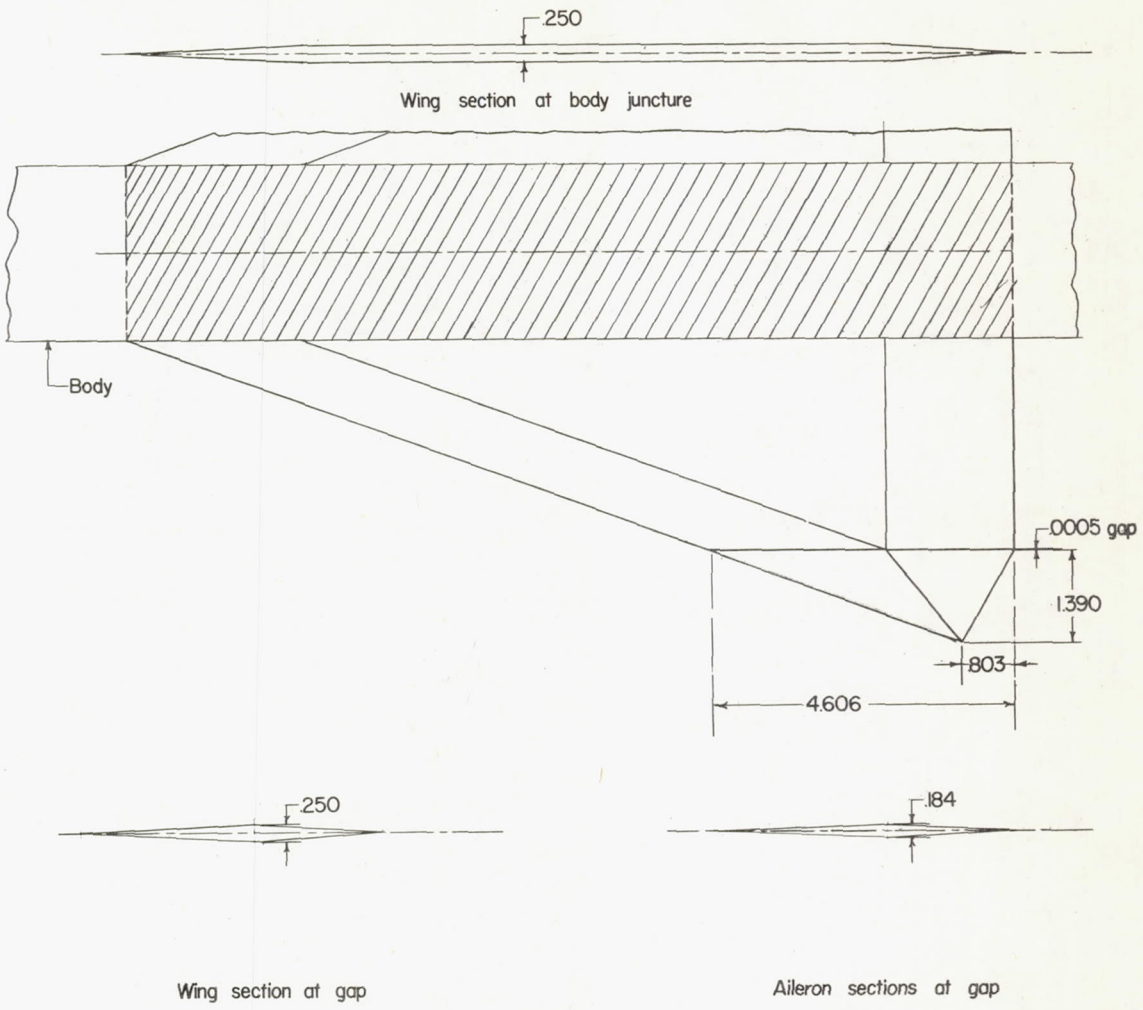
Horizontal canard



Vertical canard

(b) Details of canard control surfaces.

Figure 2.- Continued.



(c) Wing and aileron. Shaded area indicates area of body included in the total wing area.

Figure 2.- Concluded.

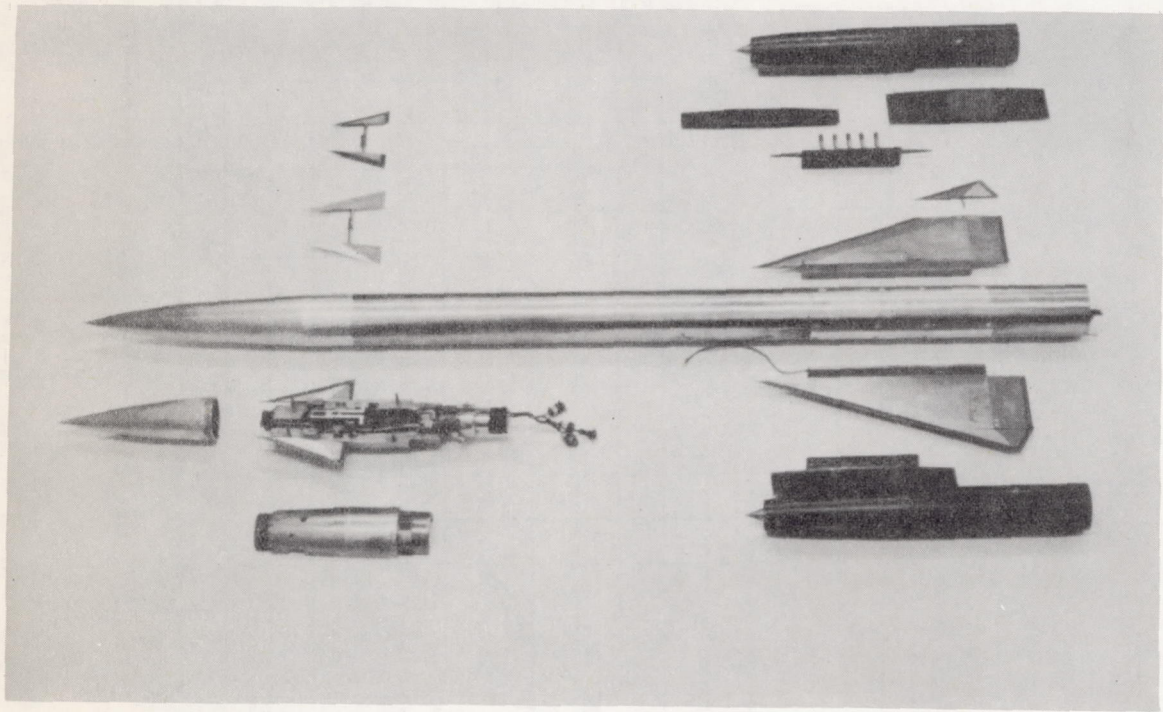


Figure 3.- Photograph of the model. L-74957

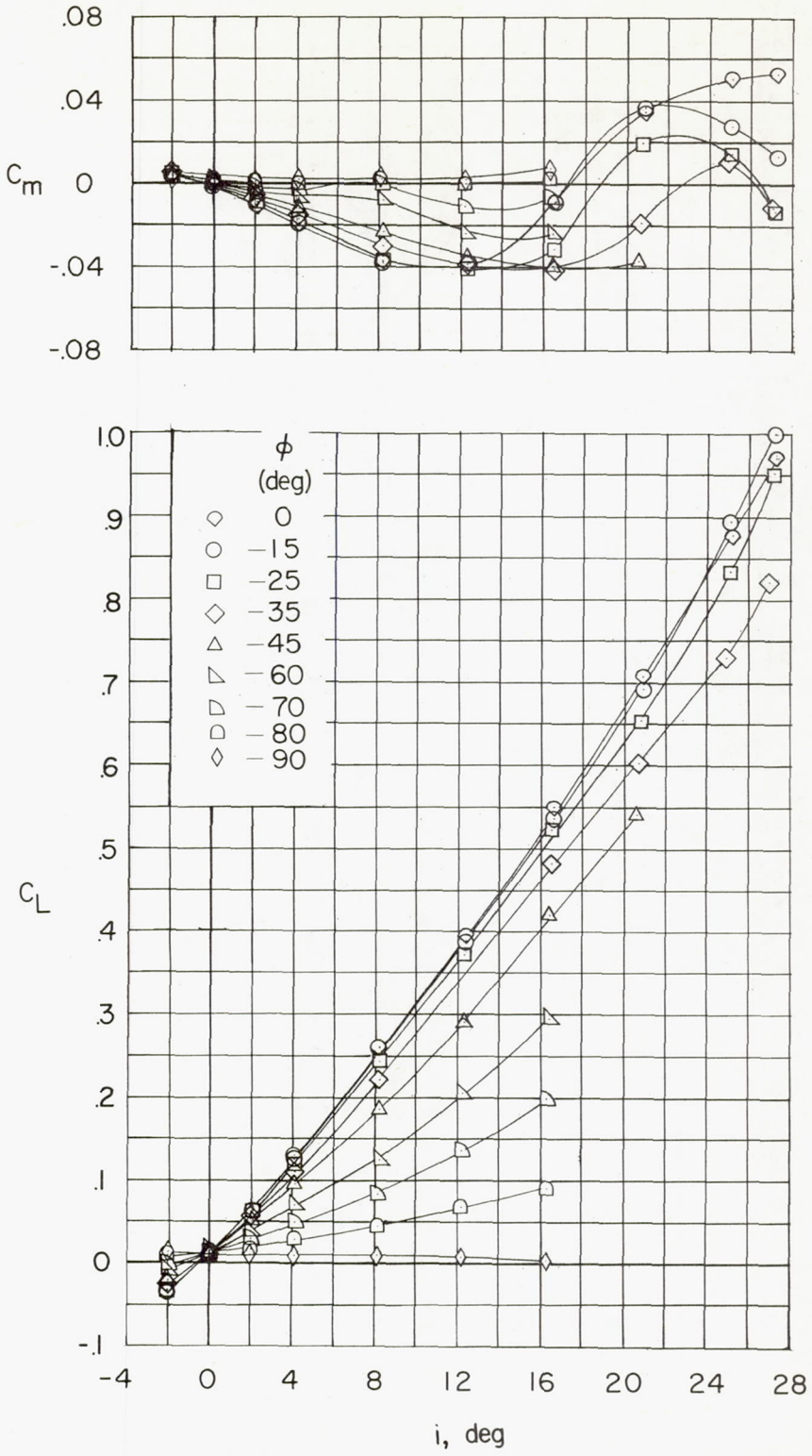


Figure 4.- The variation of the basic coefficients with incidence angle i for configuration BWCN; $\delta_H = 0^o$.

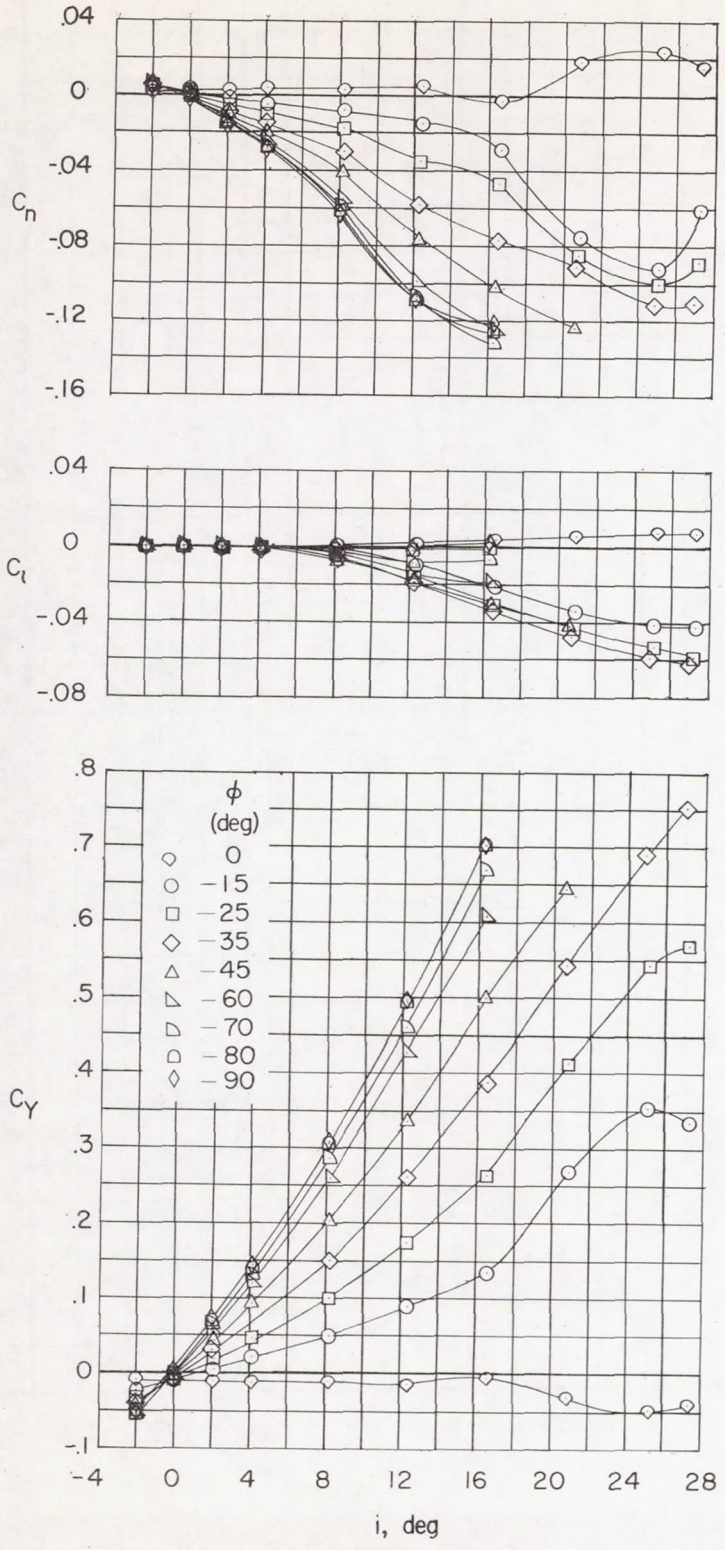


Figure 4.- Continued.

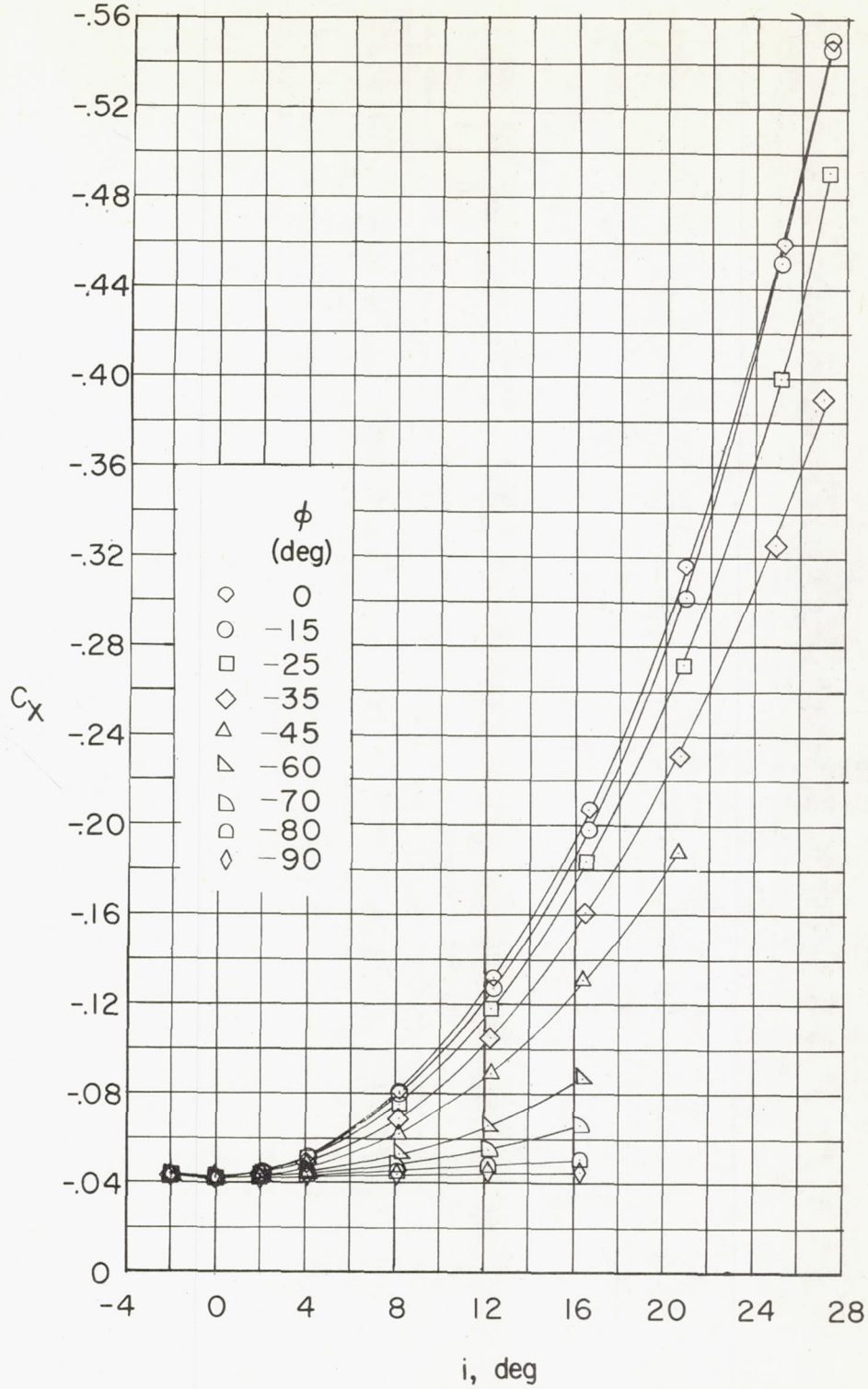


Figure 4.- Concluded.

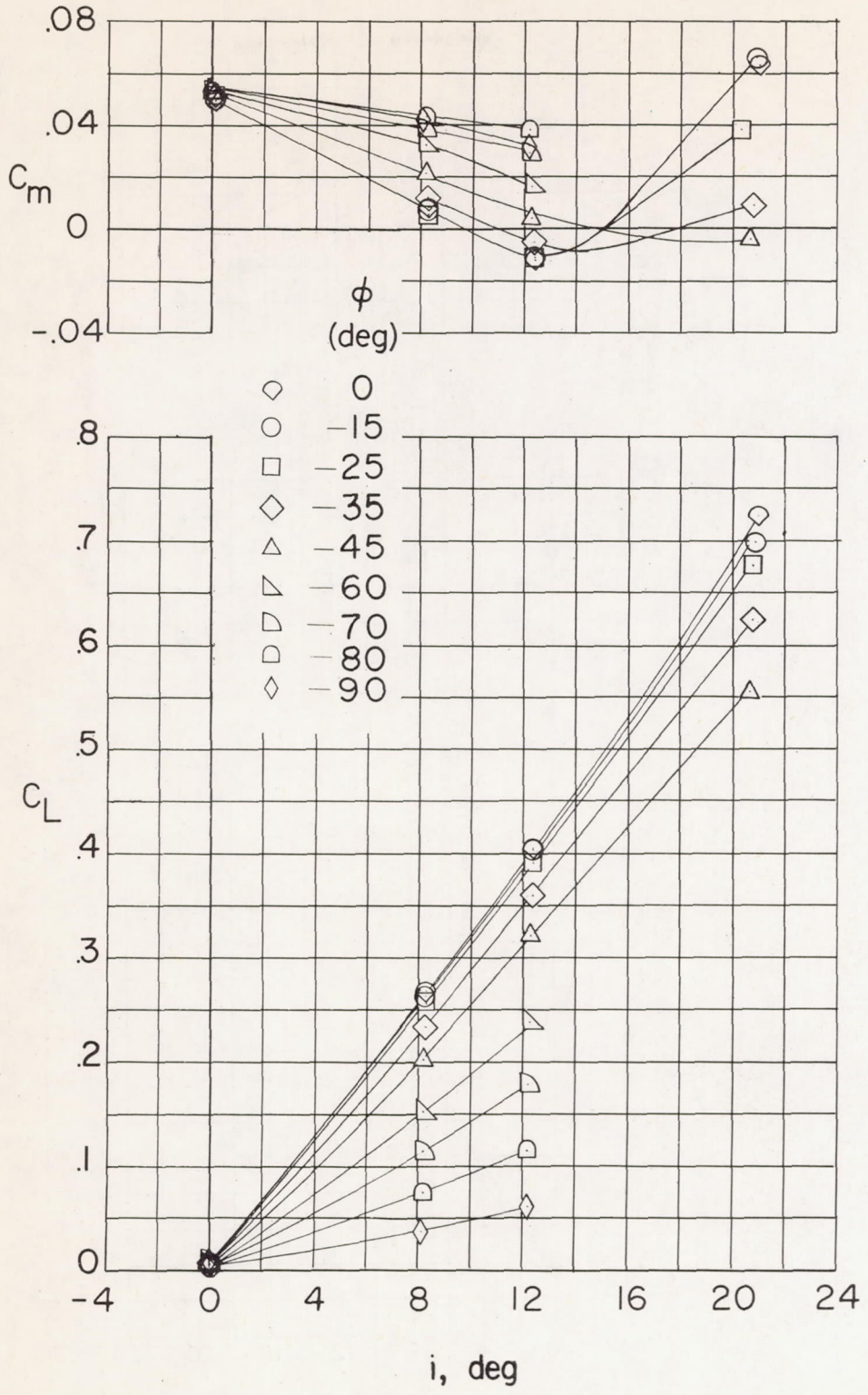


Figure 5.- The variation of the basic coefficients with incidence angle i for configuration BWCN; $\delta_H = -8^\circ$.

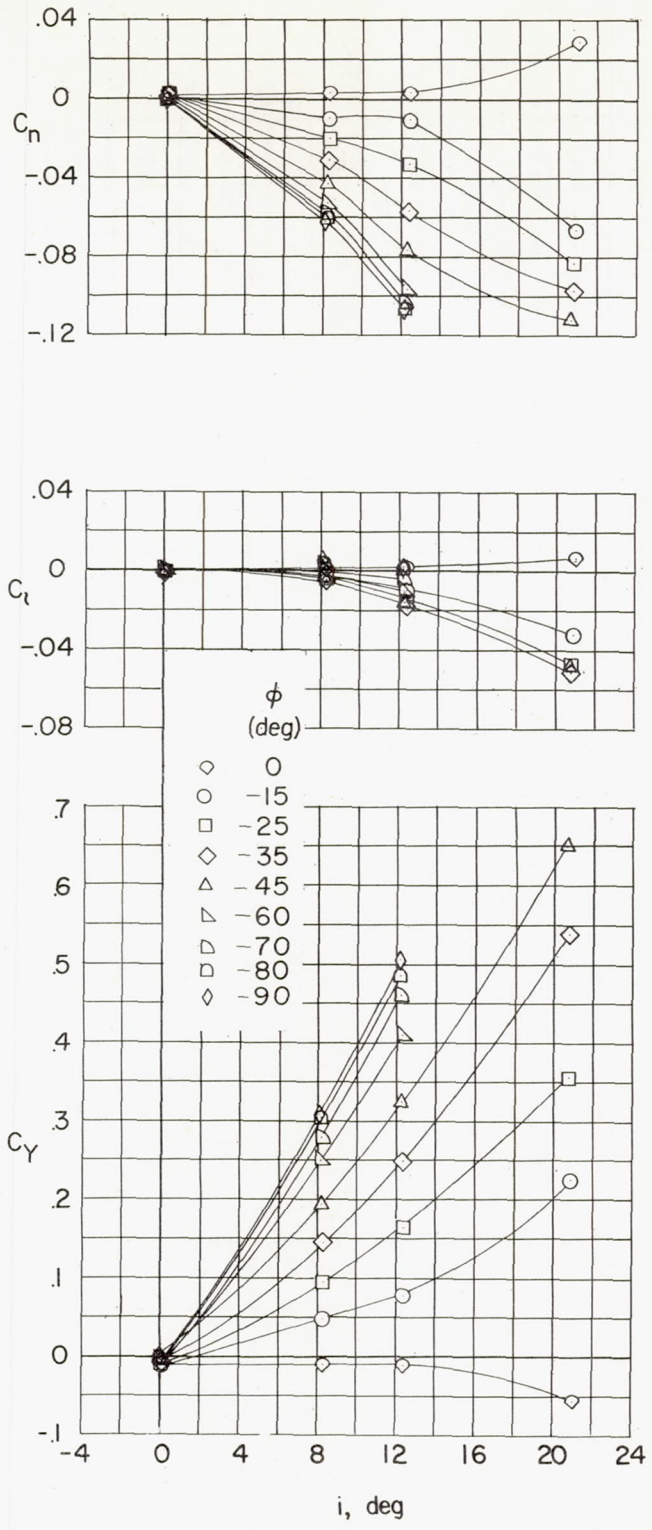


Figure 5.- Continued.

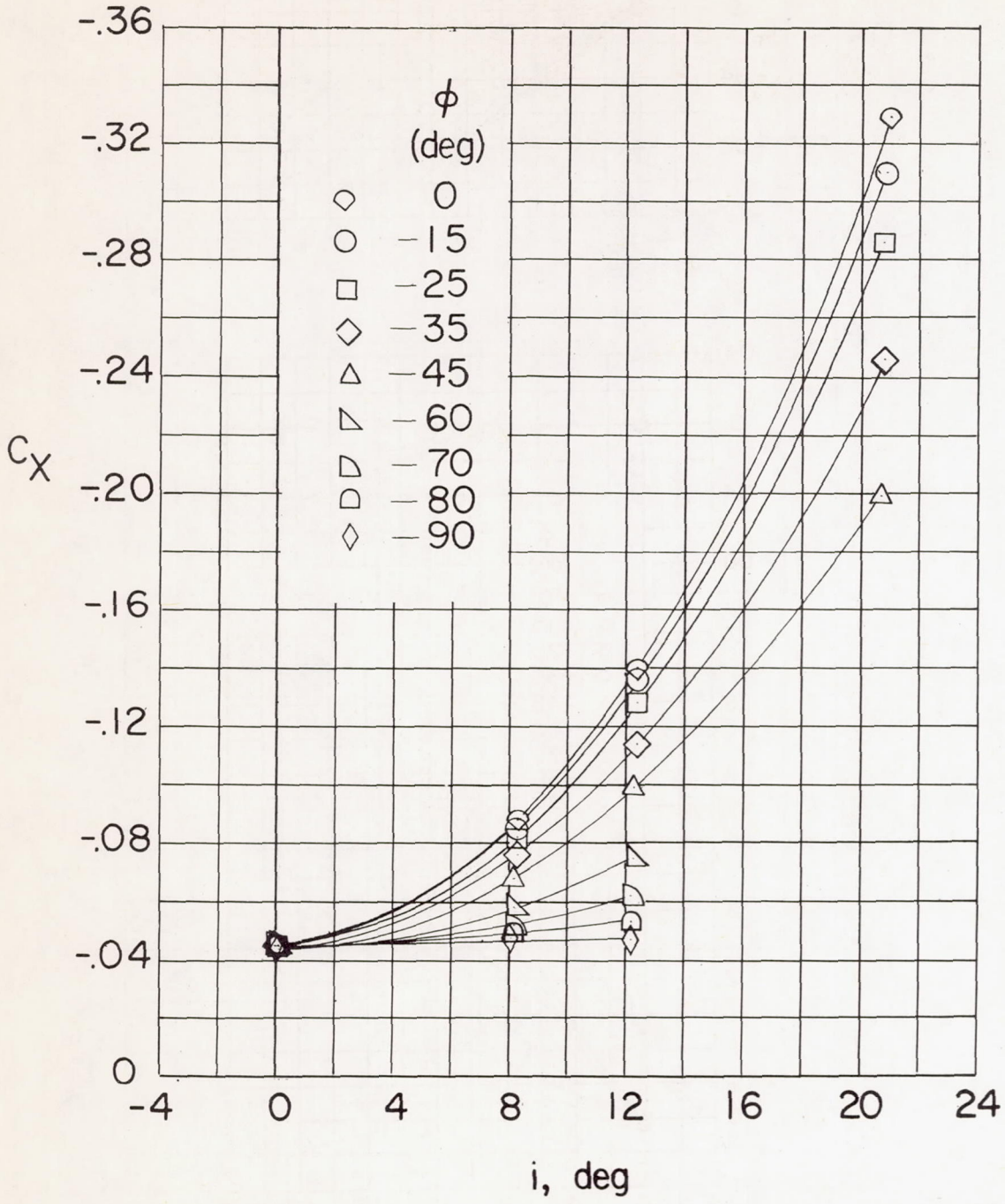


Figure 5.- Concluded.

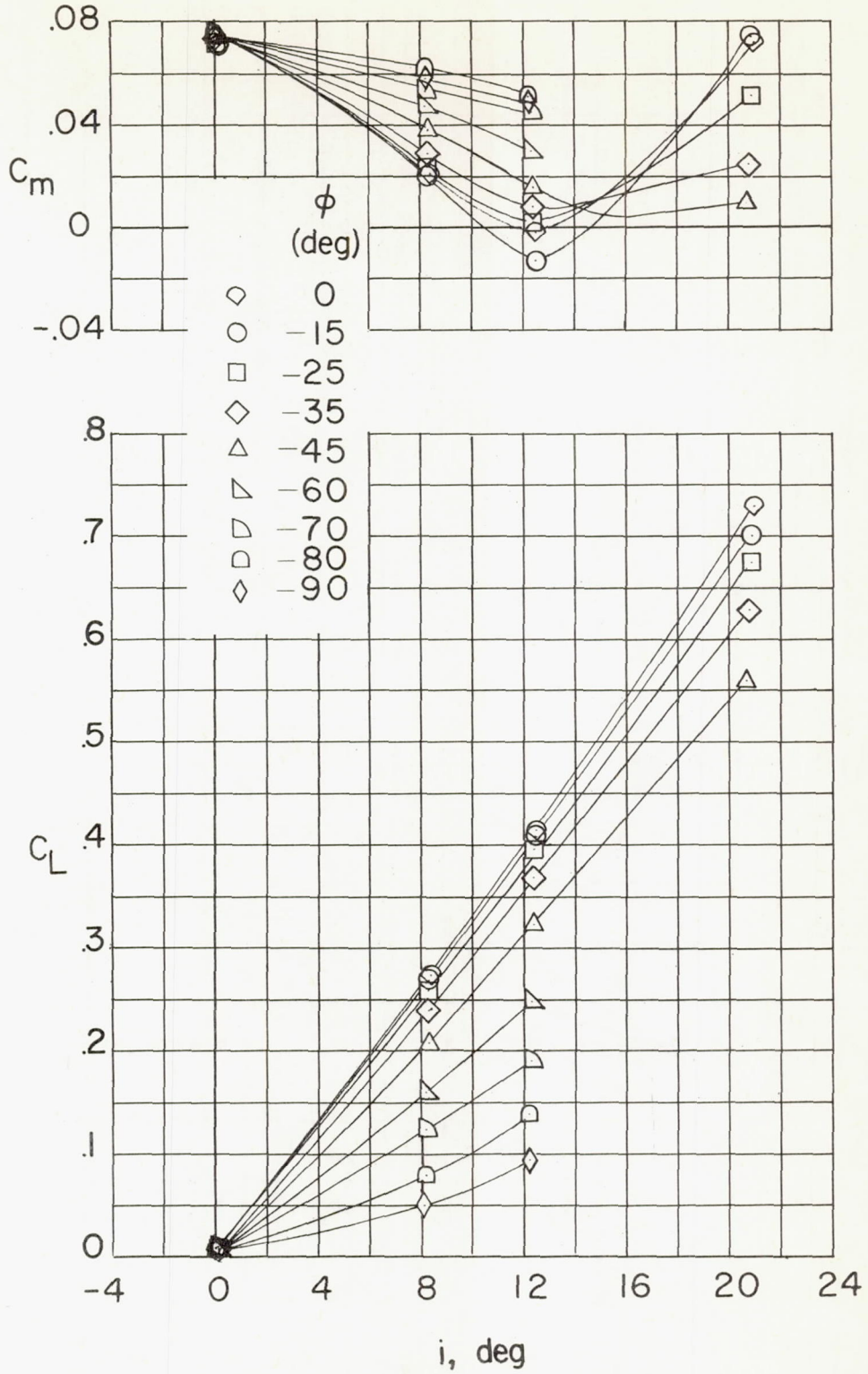


Figure 6.- The variation of the basic coefficients with incidence angle i for configuration BWCN; $\delta_H = -12^o$.

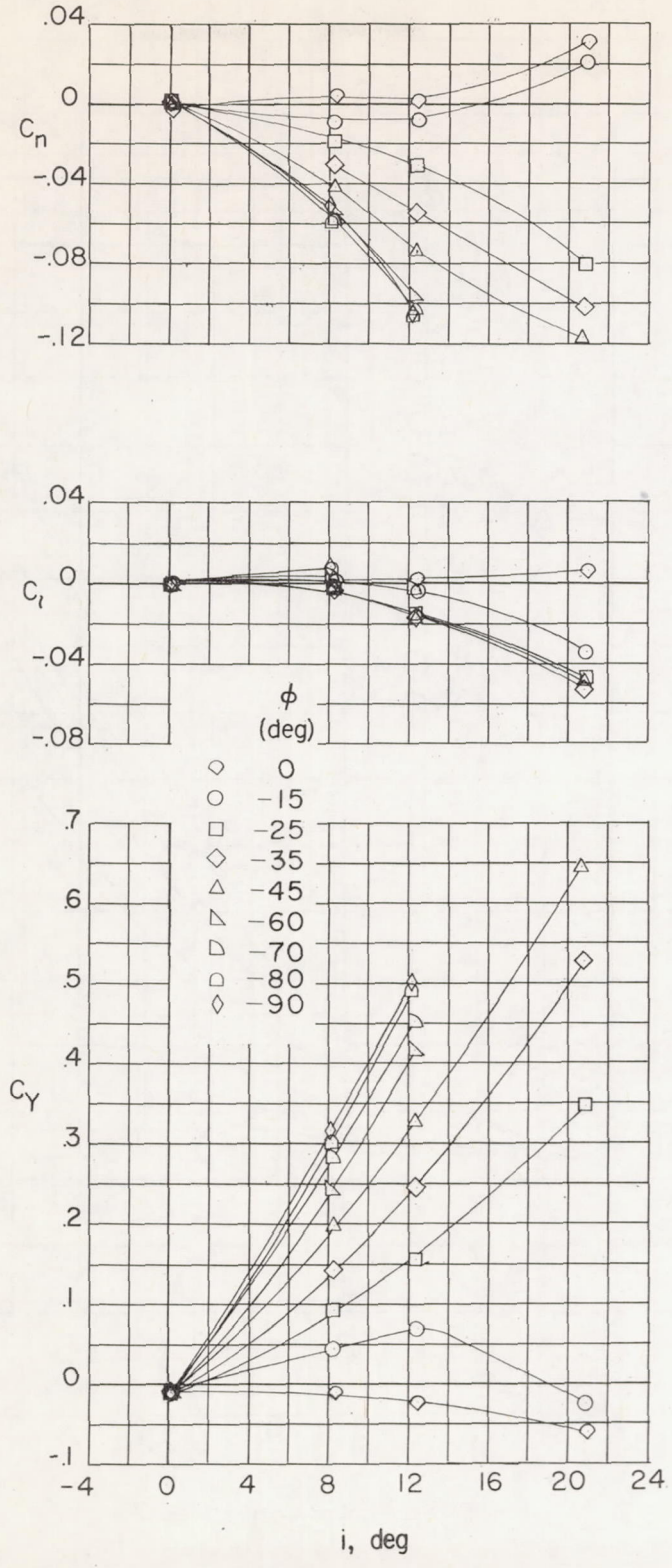


Figure 6.- Continued.

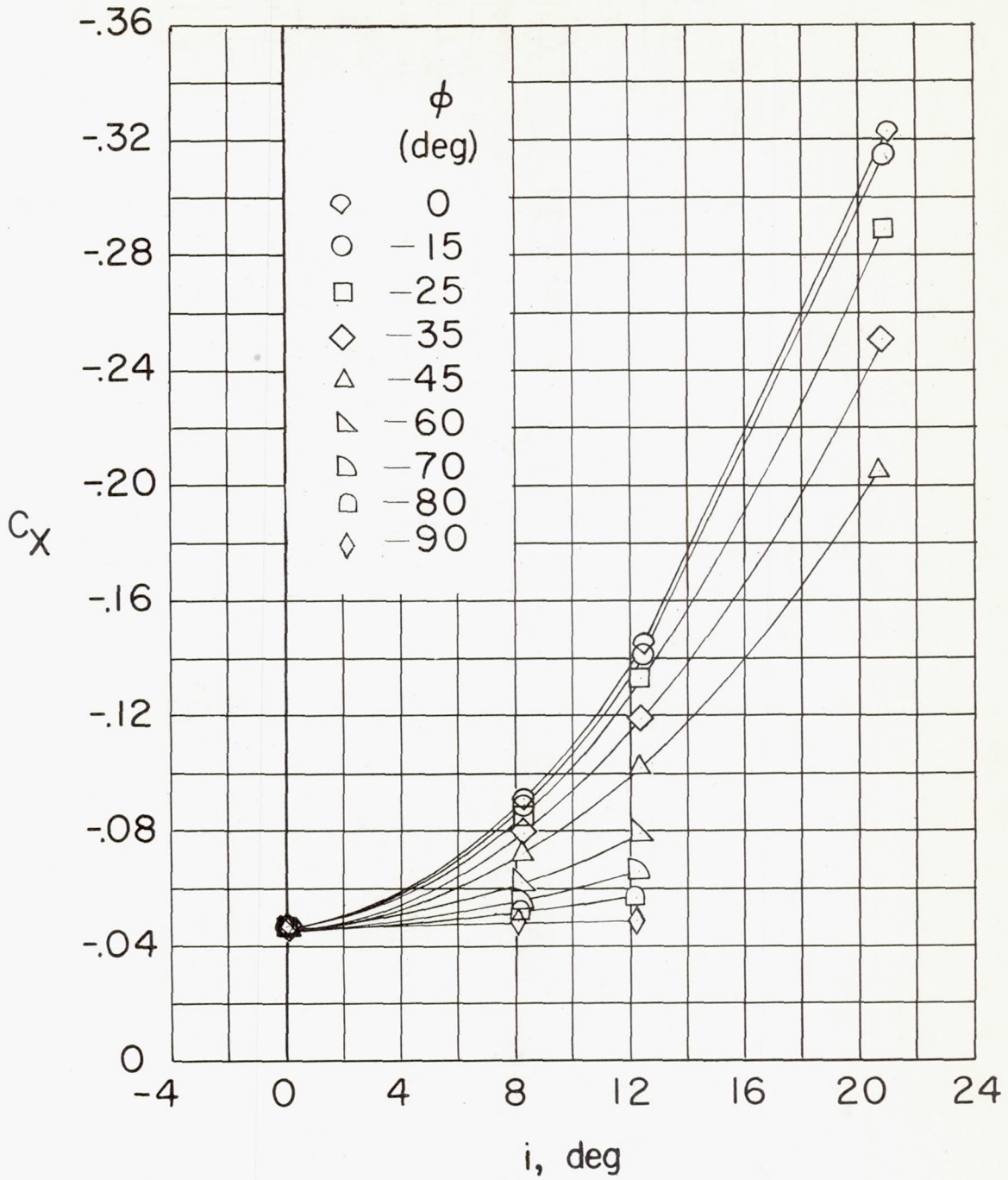


Figure 6.- Concluded.

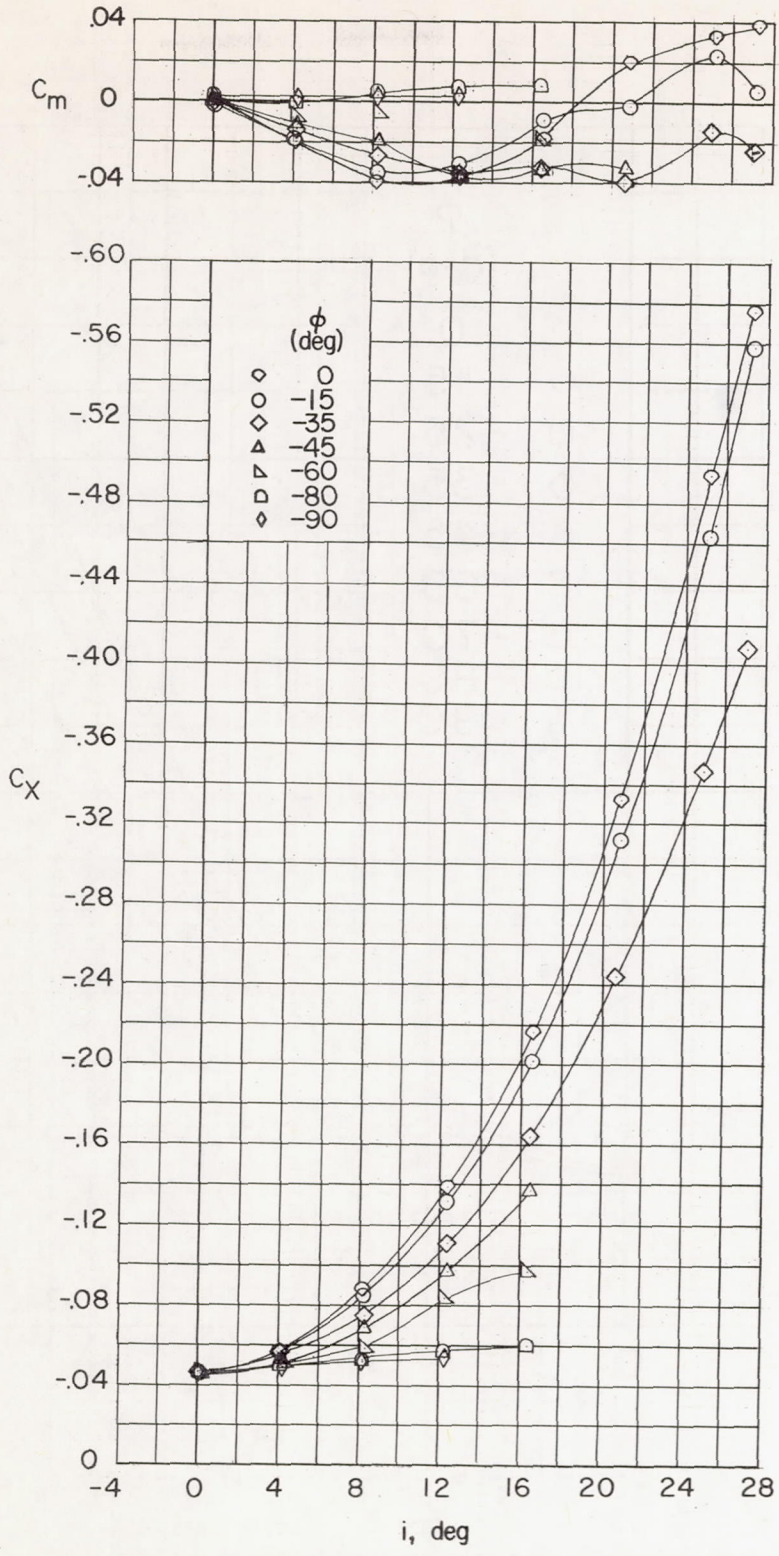


Figure 7.- The variation of basic coefficients with incidence angle i for configuration BWCN; $\delta_V = -10^o$.

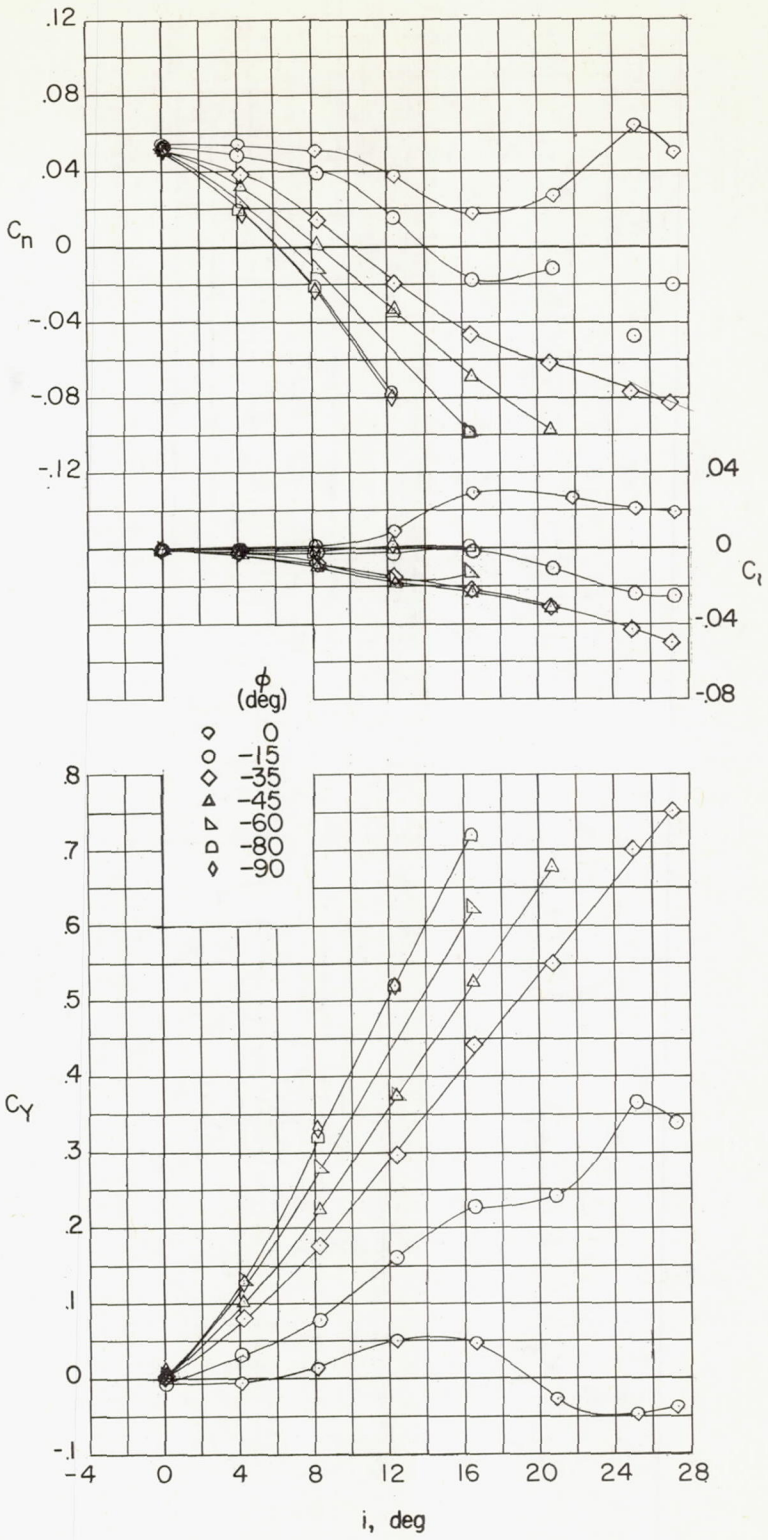


Figure 7.- Continued.

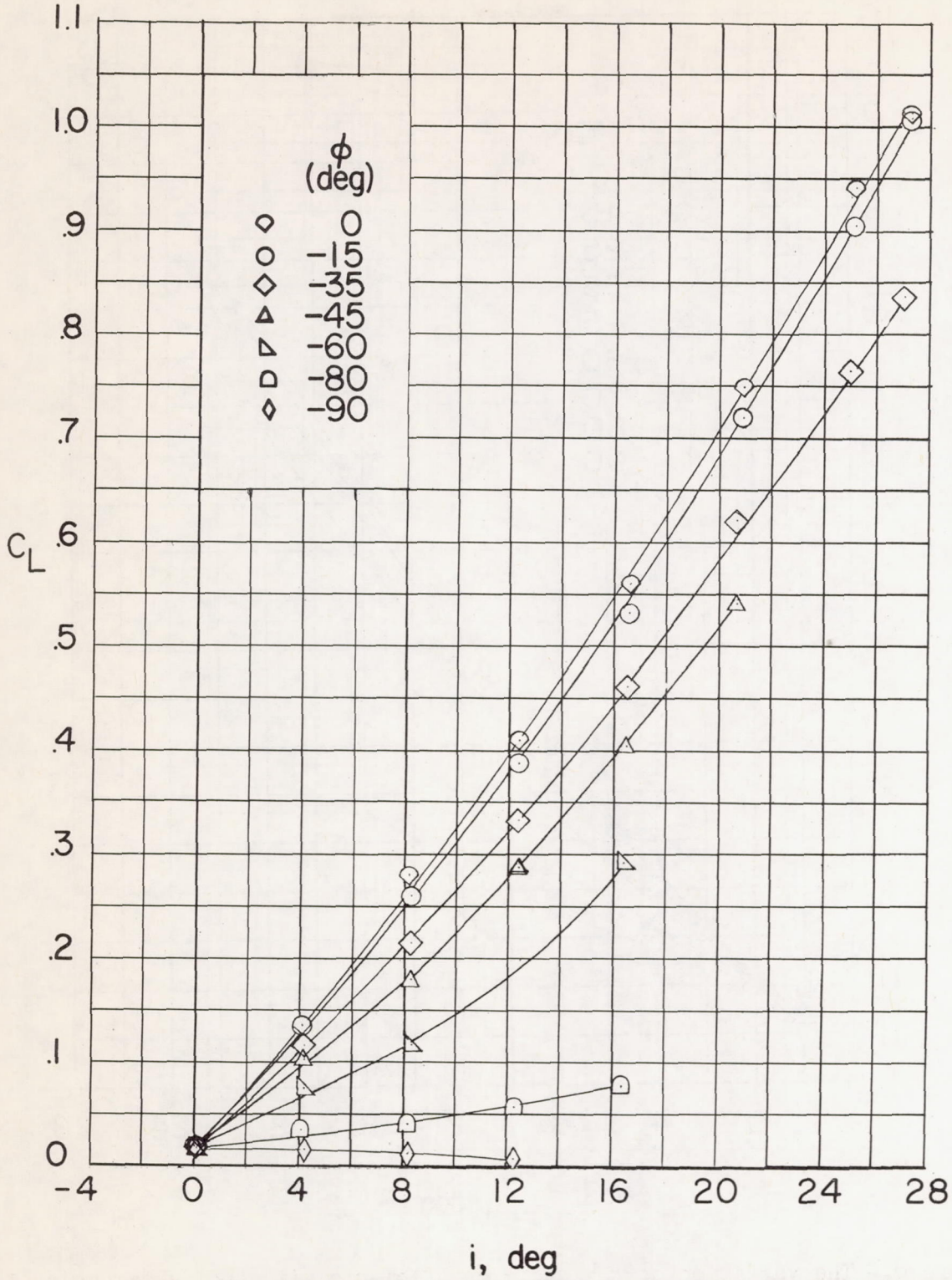


Figure 7.- Concluded.

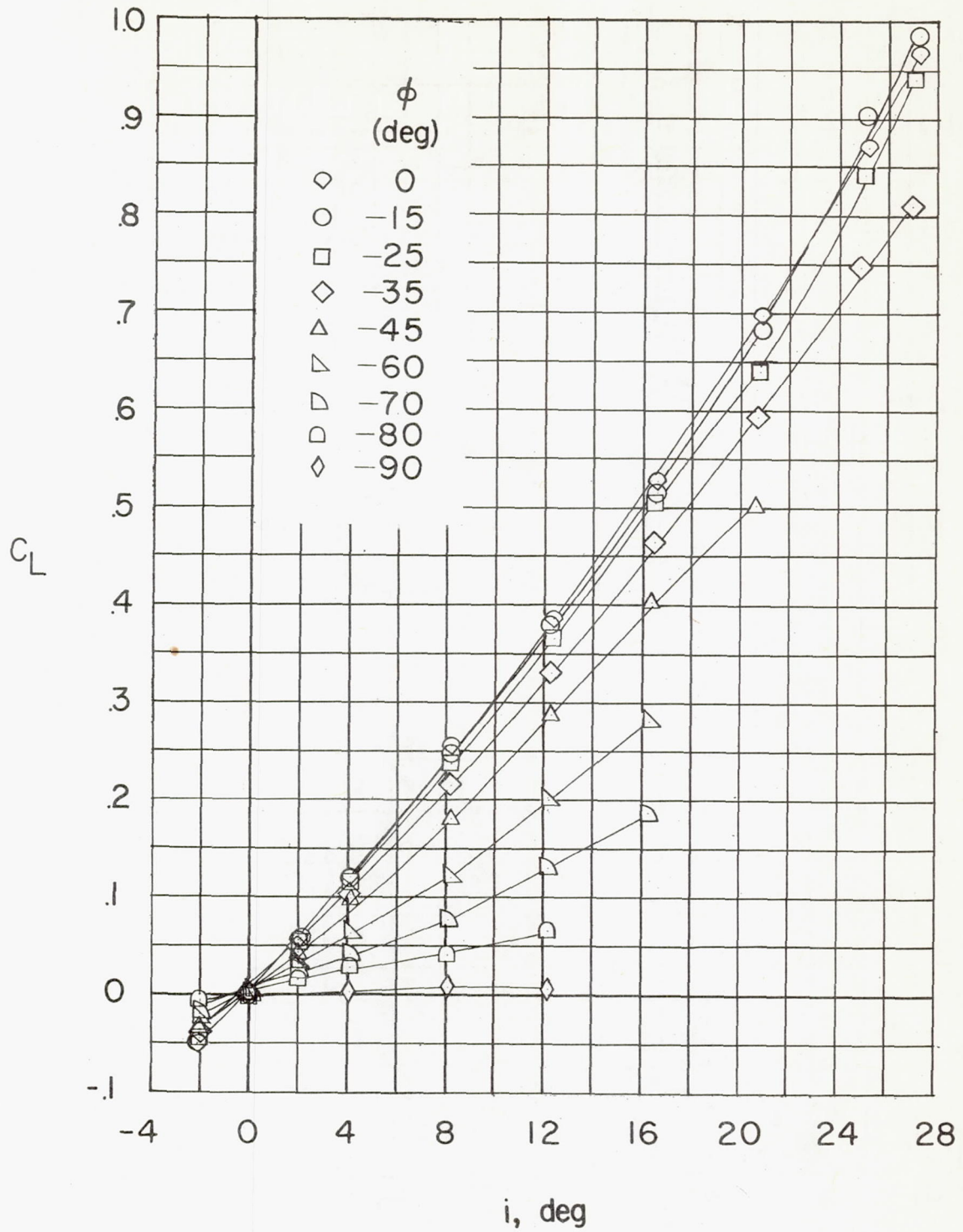


Figure 8.- The variation of the basic coefficients with incidence angle i for configuration BWCN; $\delta_{a_L} = 10^\circ$; $\delta_{a_R} = -10^\circ$.

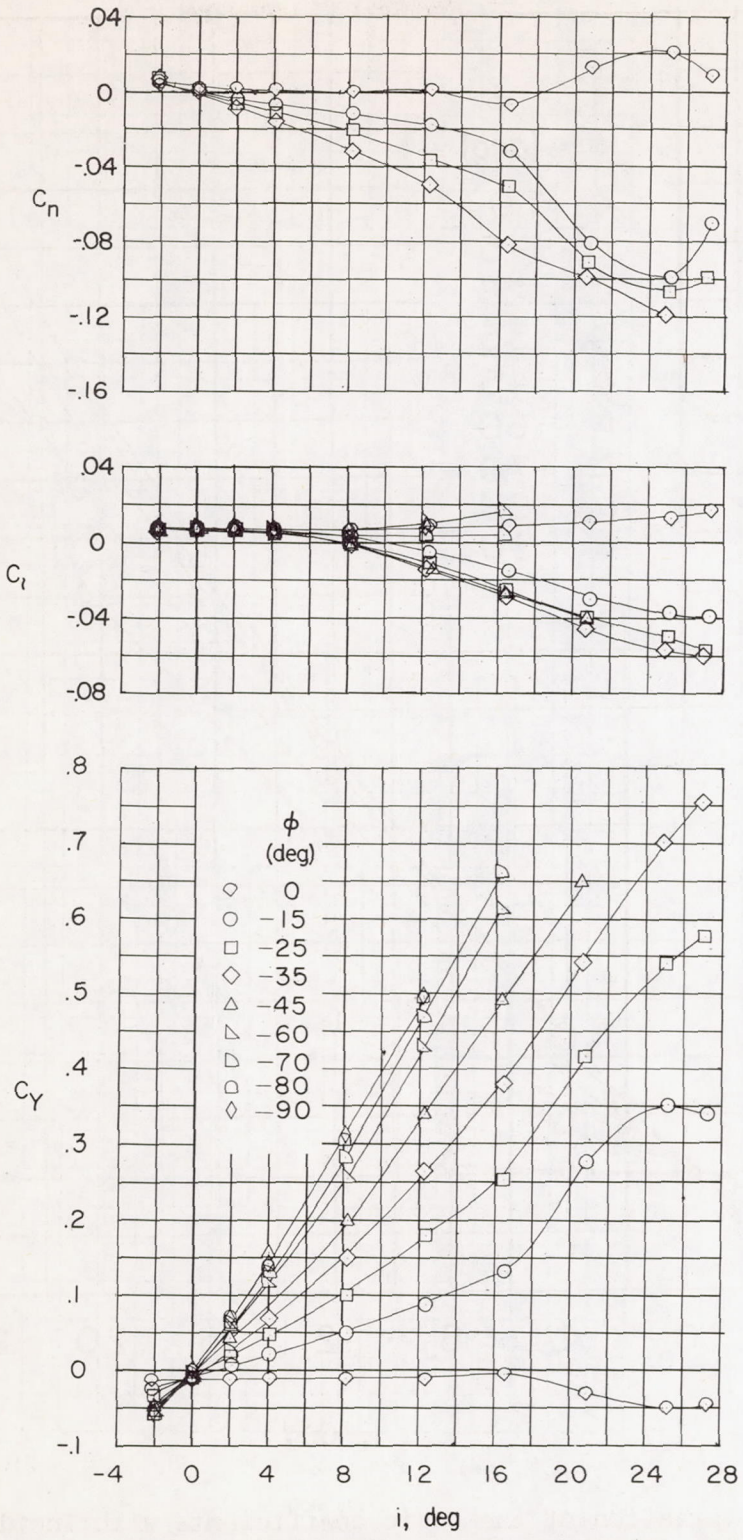


Figure 8.- Continued.

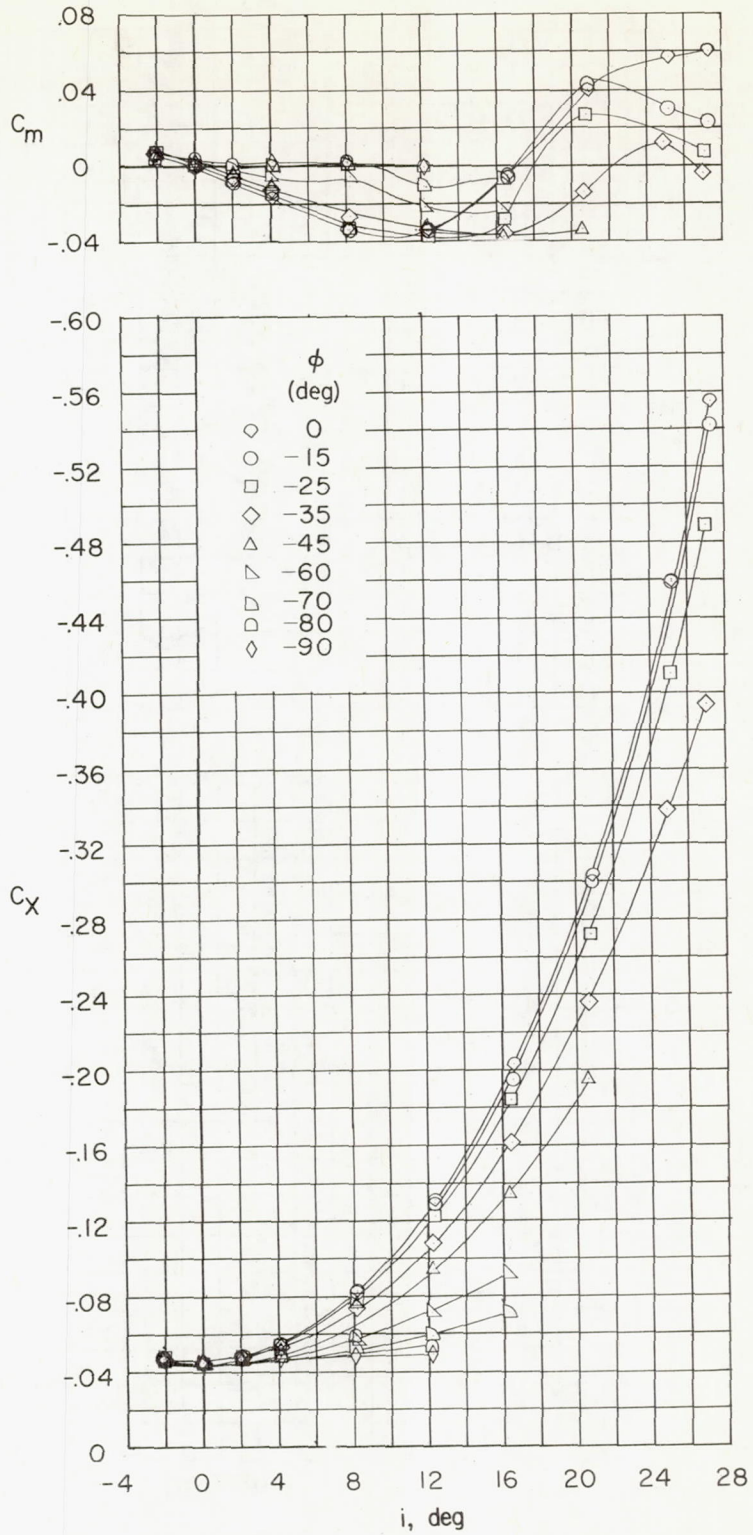


Figure 8.- Concluded.

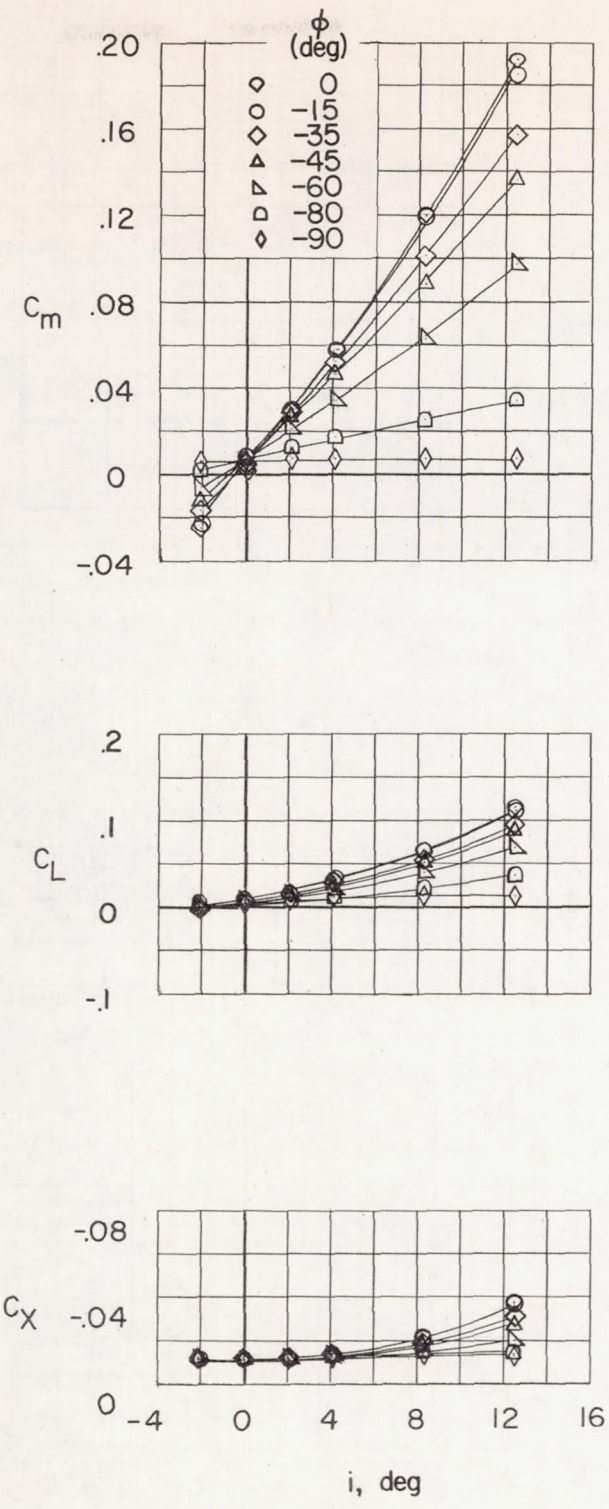


Figure 9.- The variation of the basic coefficients with incidence angle i for configuration BC; $\delta_H = 0^o$.

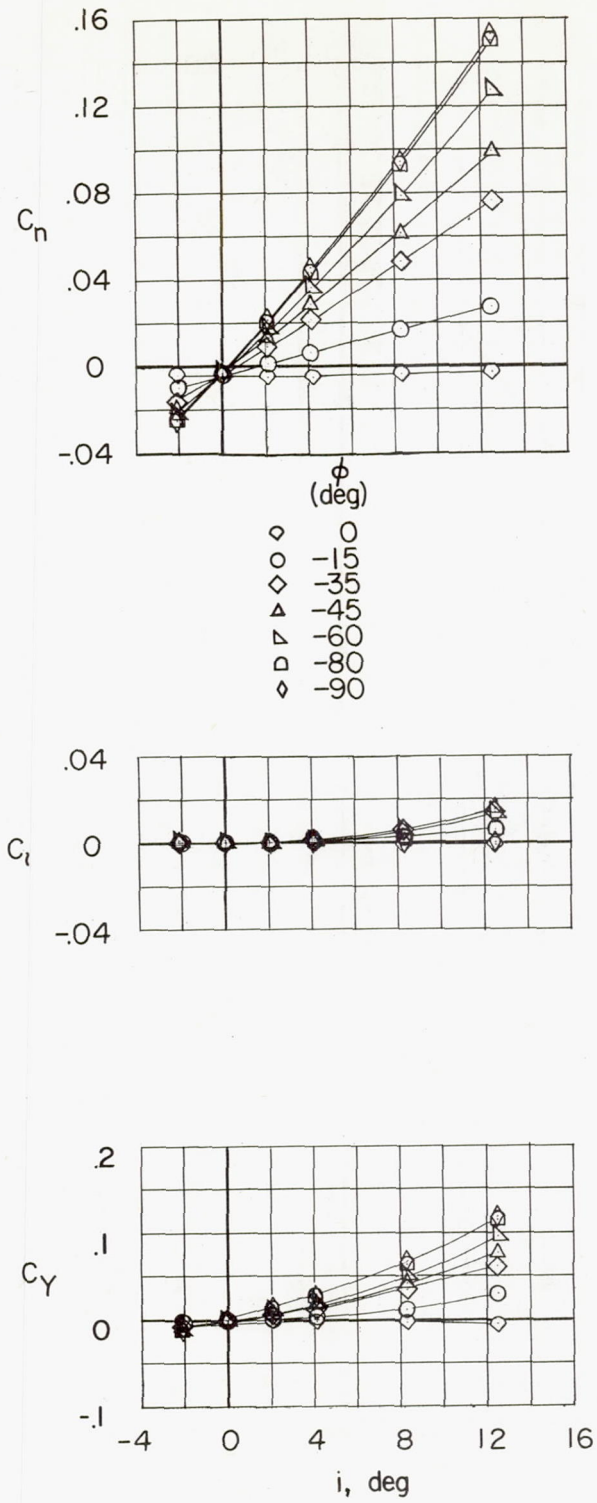


Figure 9.- Concluded.

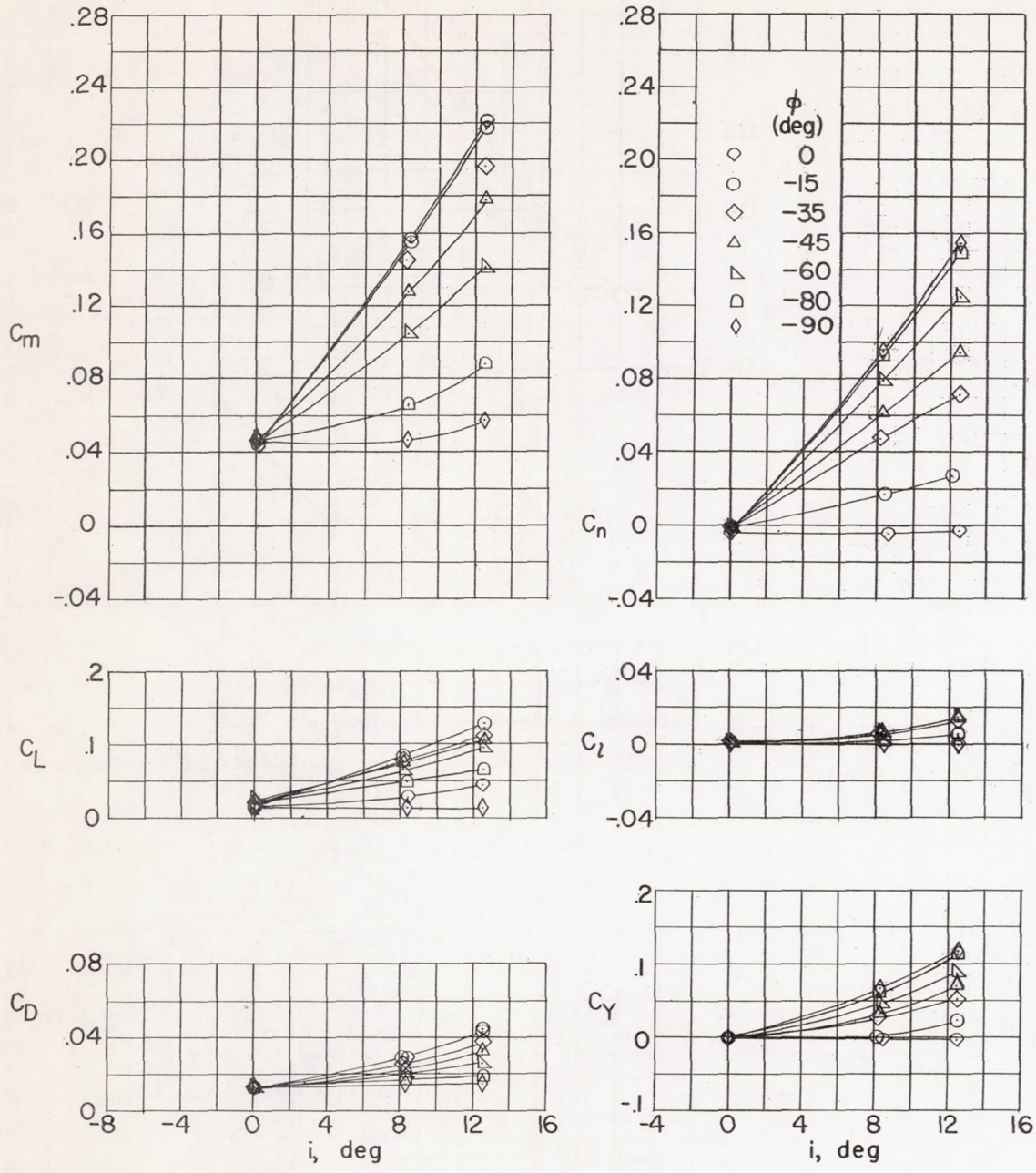


Figure 10.- The variation of the basic coefficients with incidence angle i for configuration BC; $\delta_H = -8^\circ$.

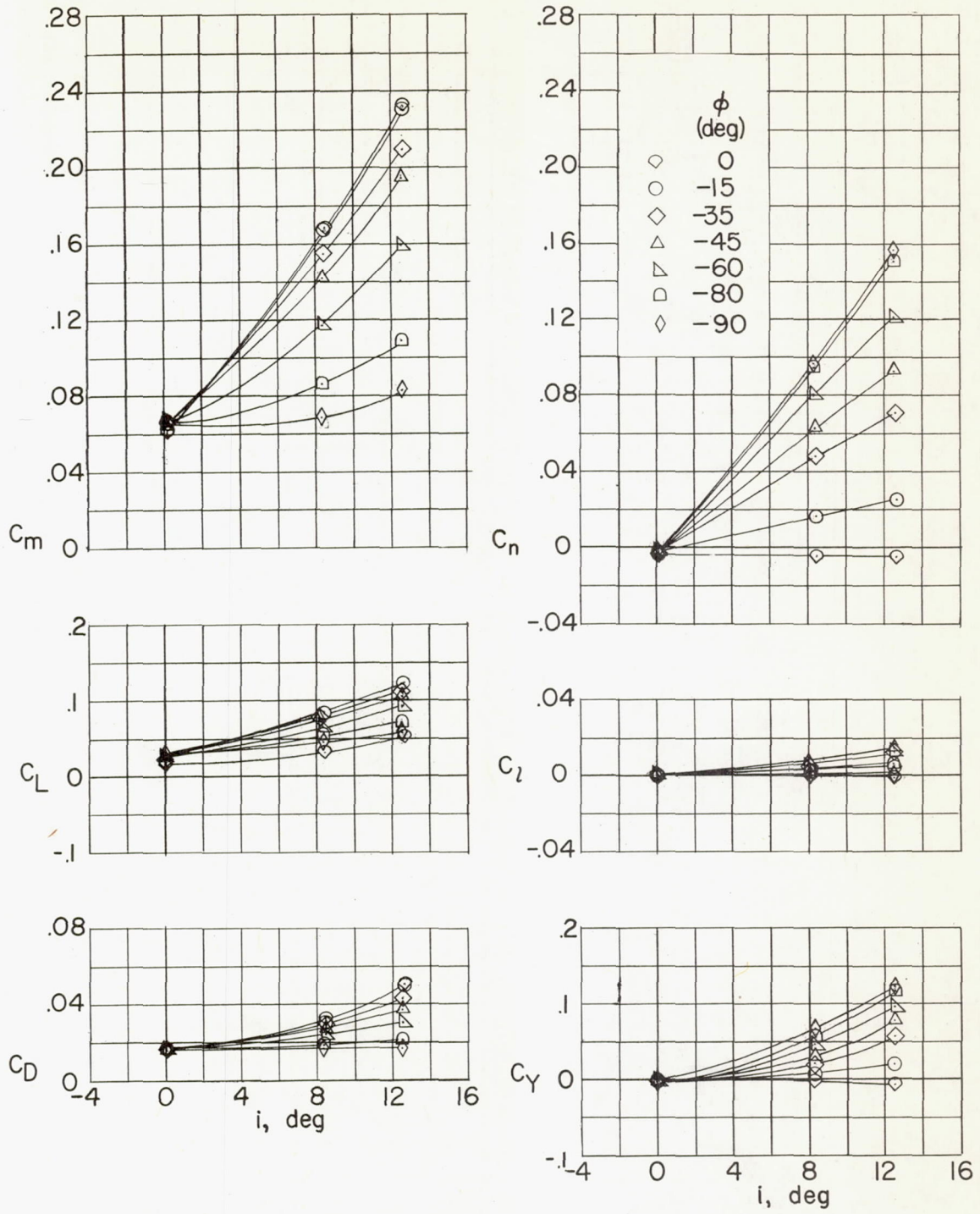


Figure 11.- The variation of the basic coefficients with incidence angle i for configuration BC; $\delta_H = -12^\circ$.

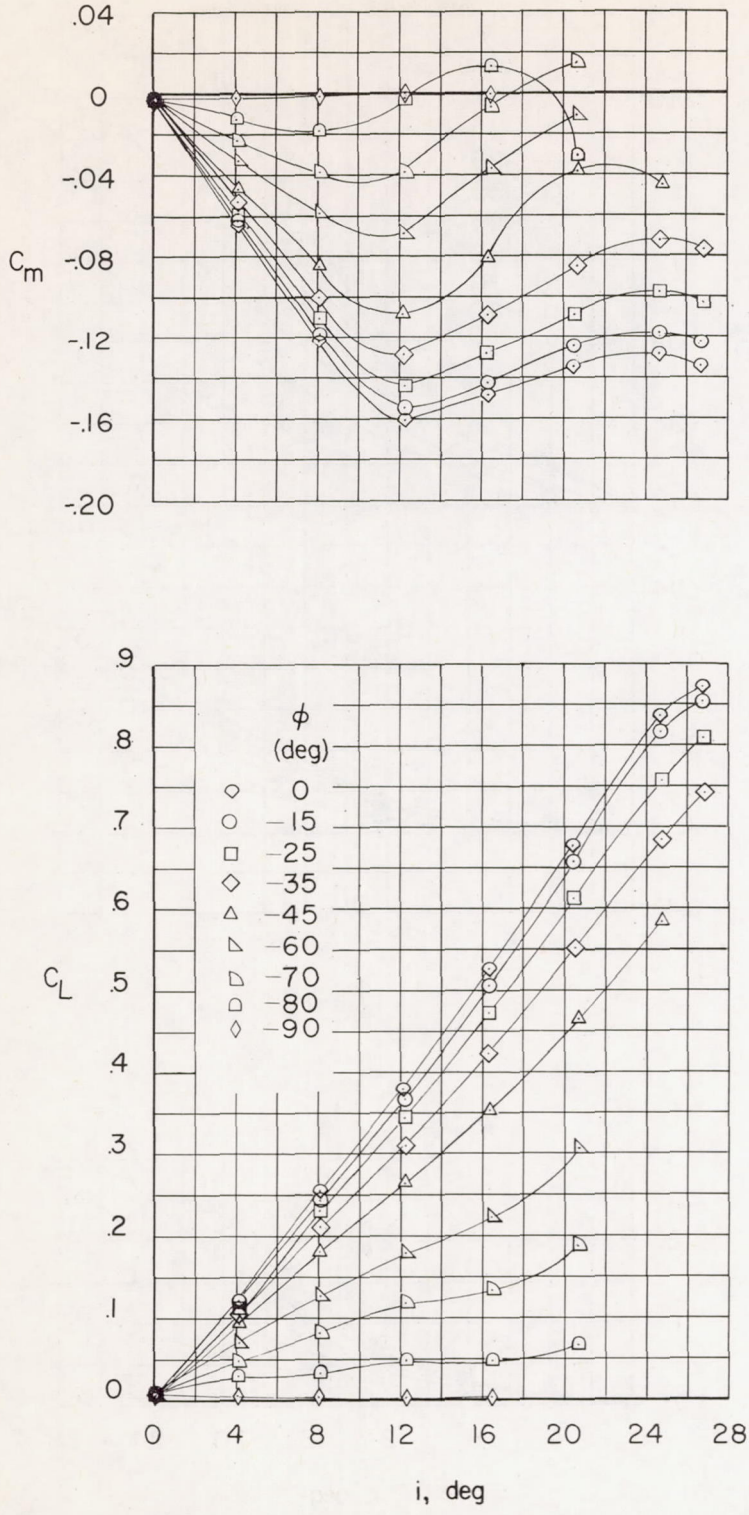


Figure 12.- The variation of the basic coefficients with incidence angle i for configuration BW.

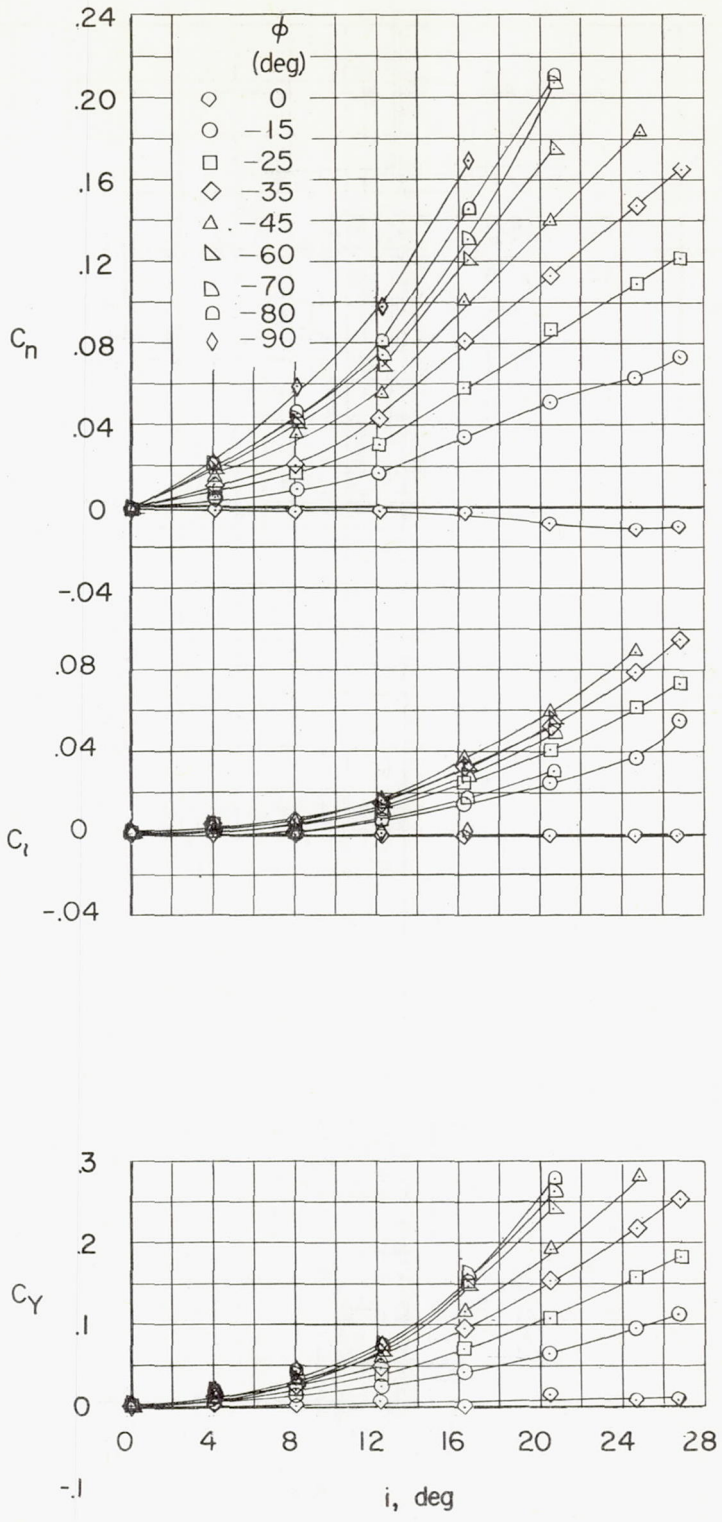


Figure 12.- Continued.

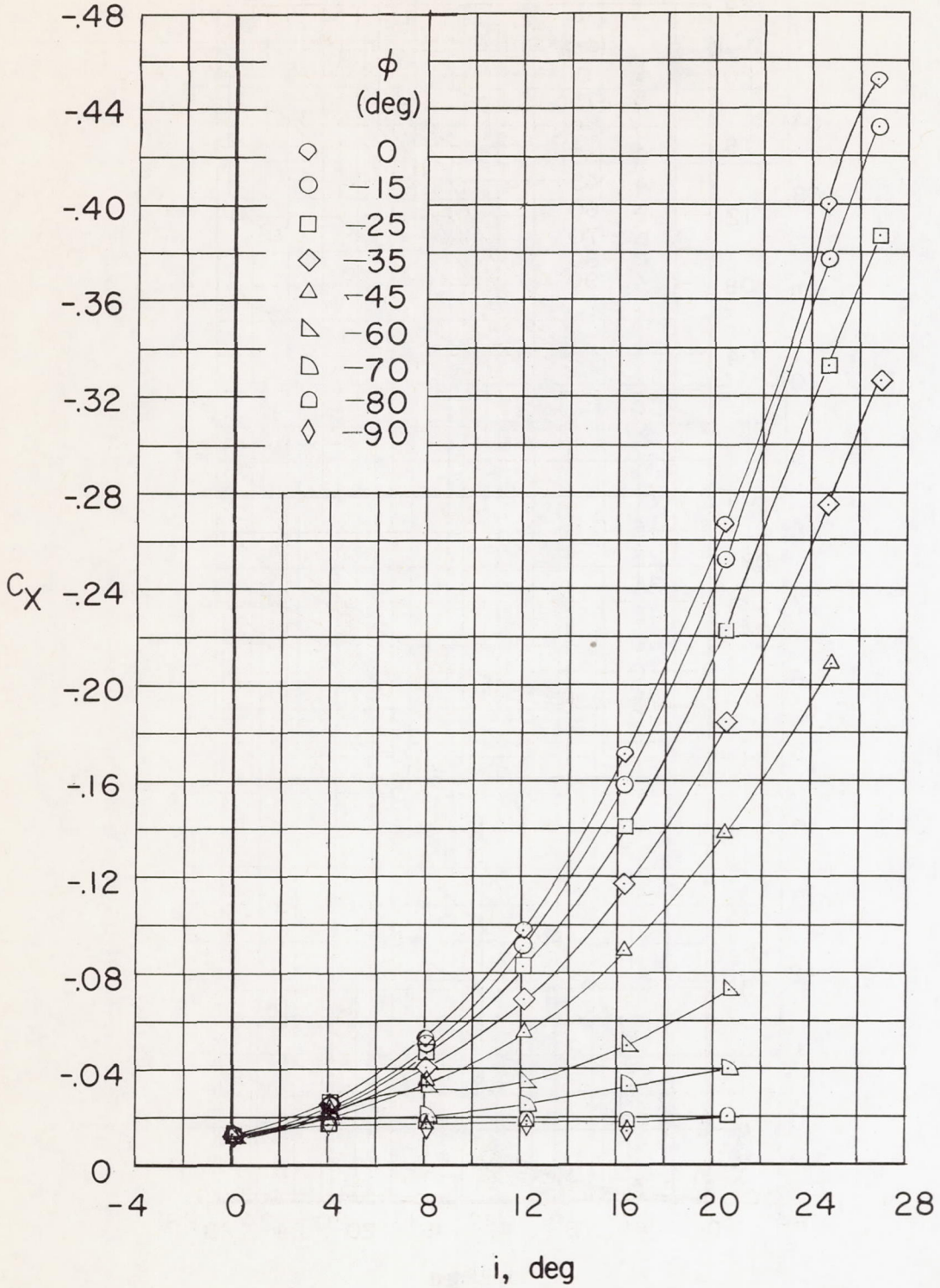
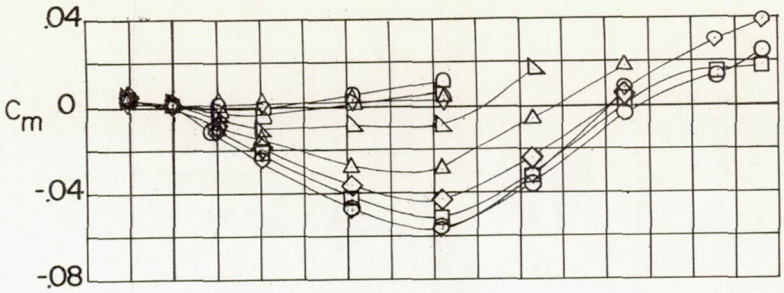


Figure 12.- Concluded.



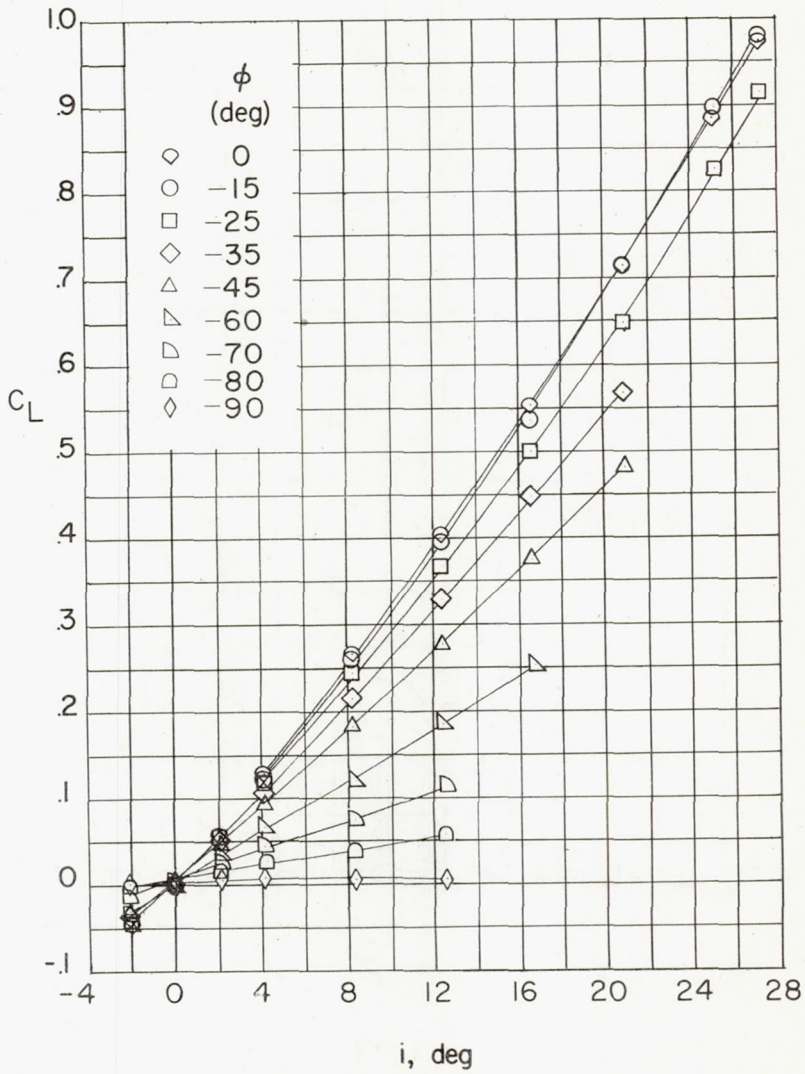


Figure 13.- The variation of the basic coefficients with incidence angle i for configuration BWC; $\delta_H = 0^\circ$.

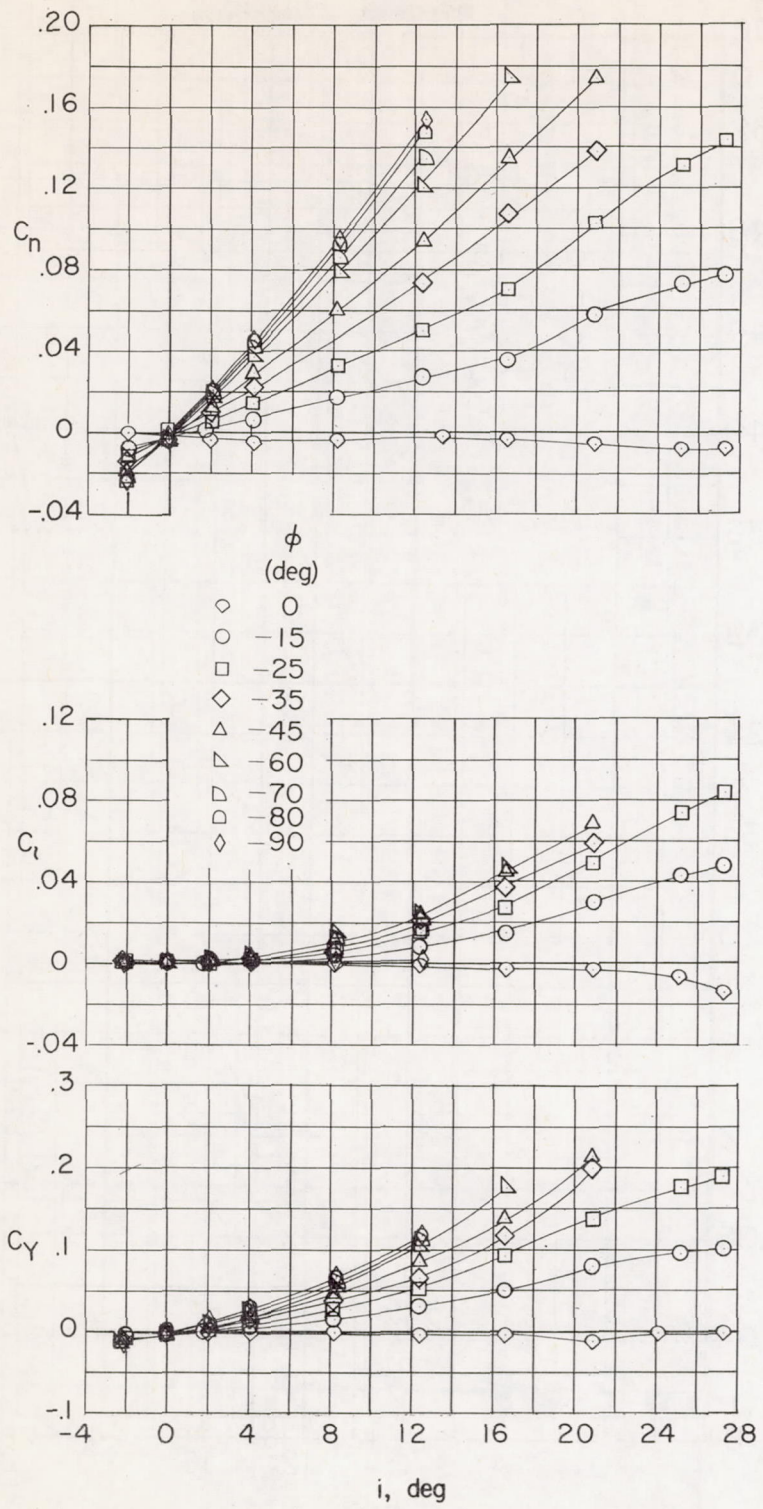


Figure 13.- Continued.

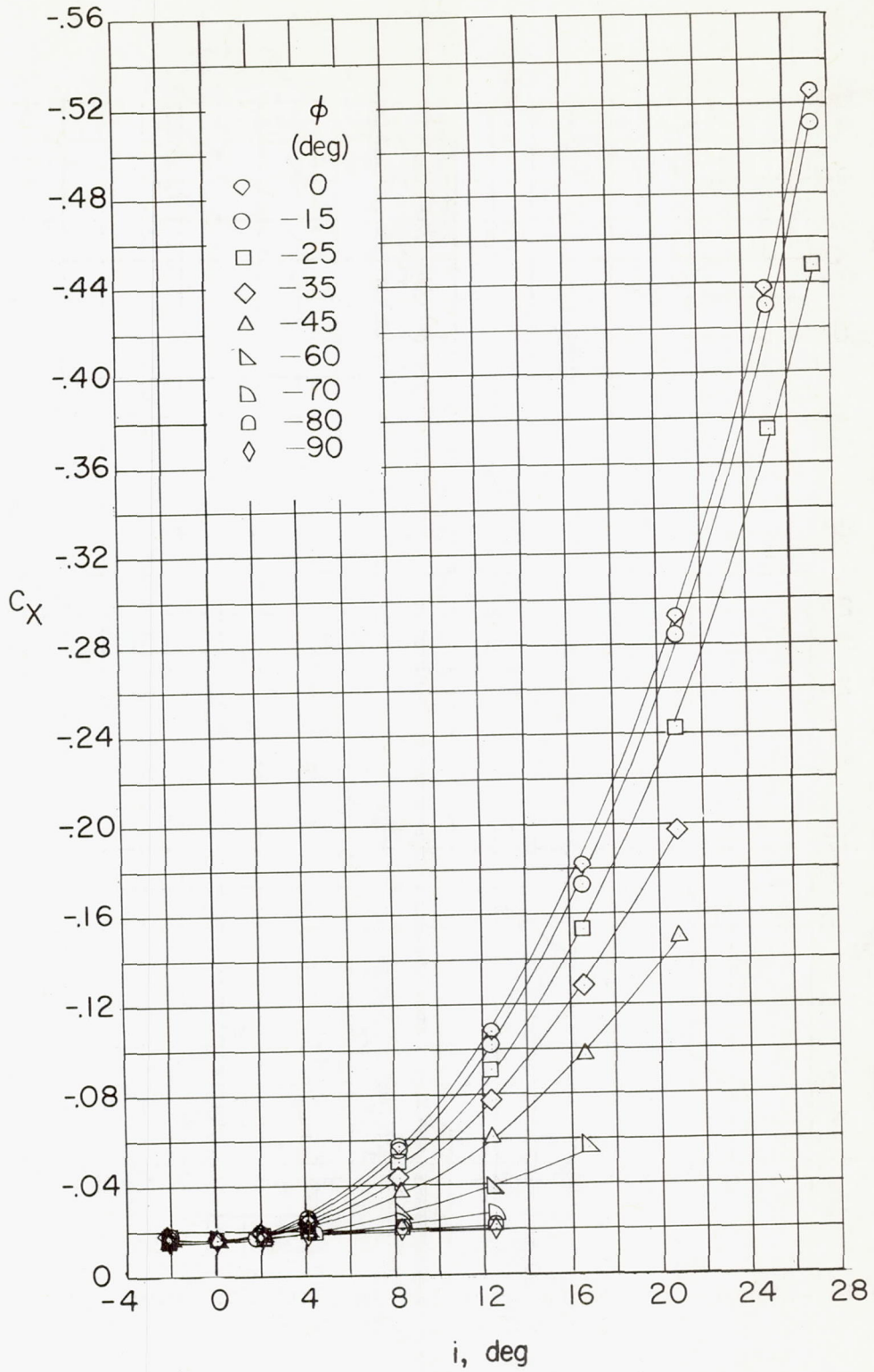


Figure 13.- Concluded.

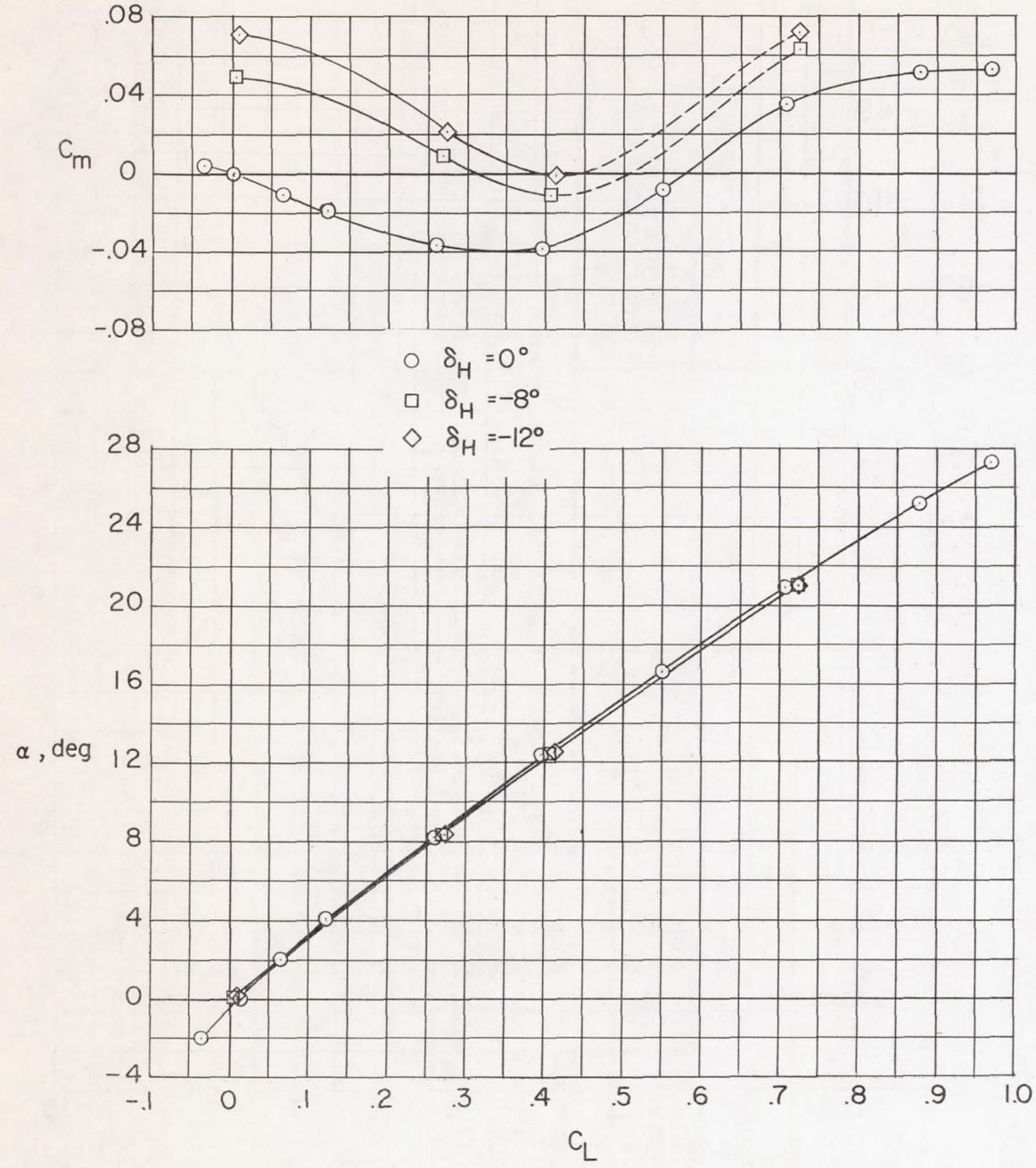


Figure 14.- Aerodynamic characteristics in pitch for several constant control deflections; $\beta = 0^\circ$.

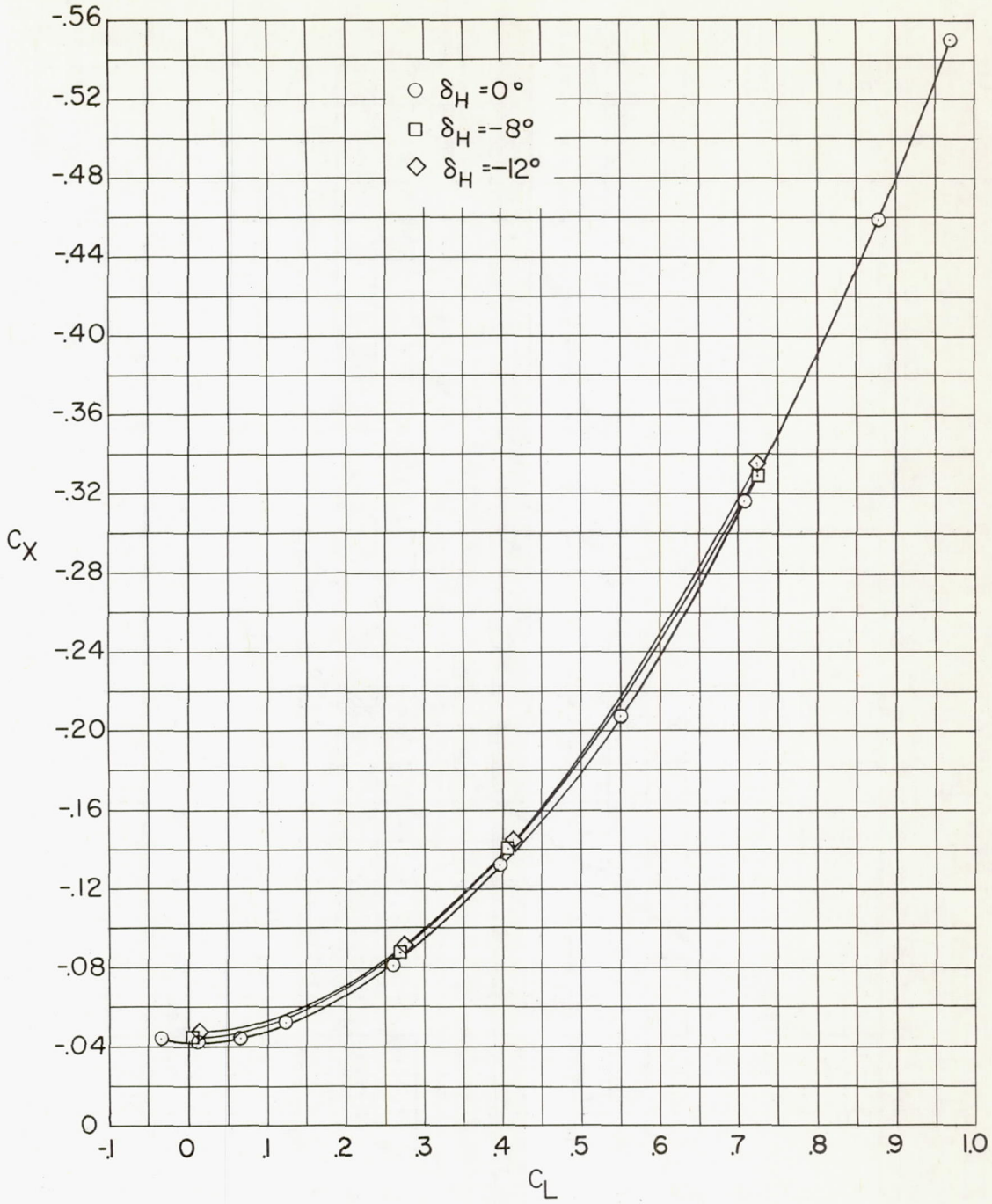


Figure 14.- Concluded.

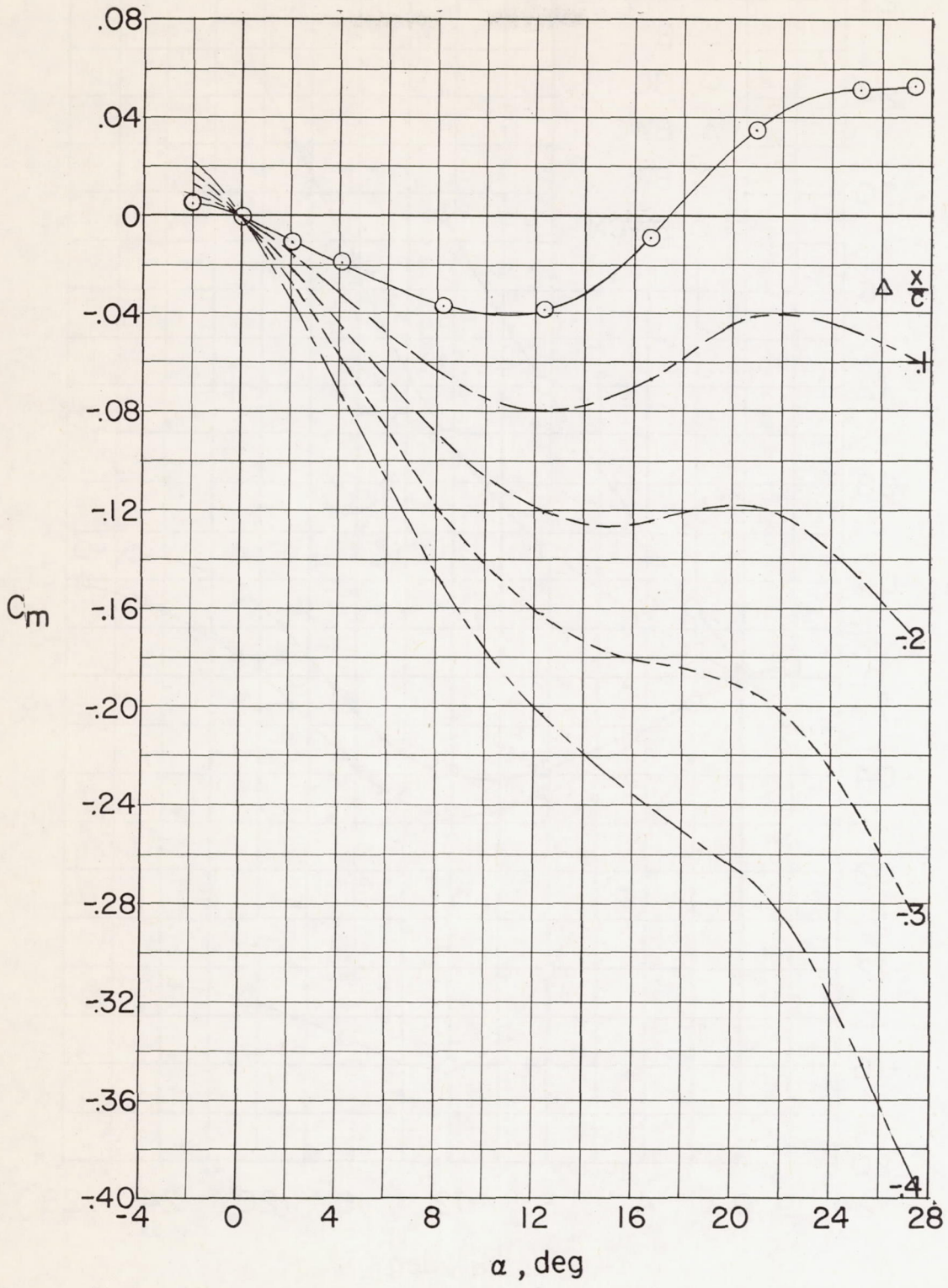


Figure 15.- Effect of center-of-gravity location on the aerodynamic characteristics in pitch; $\beta = 0^{\circ}$.

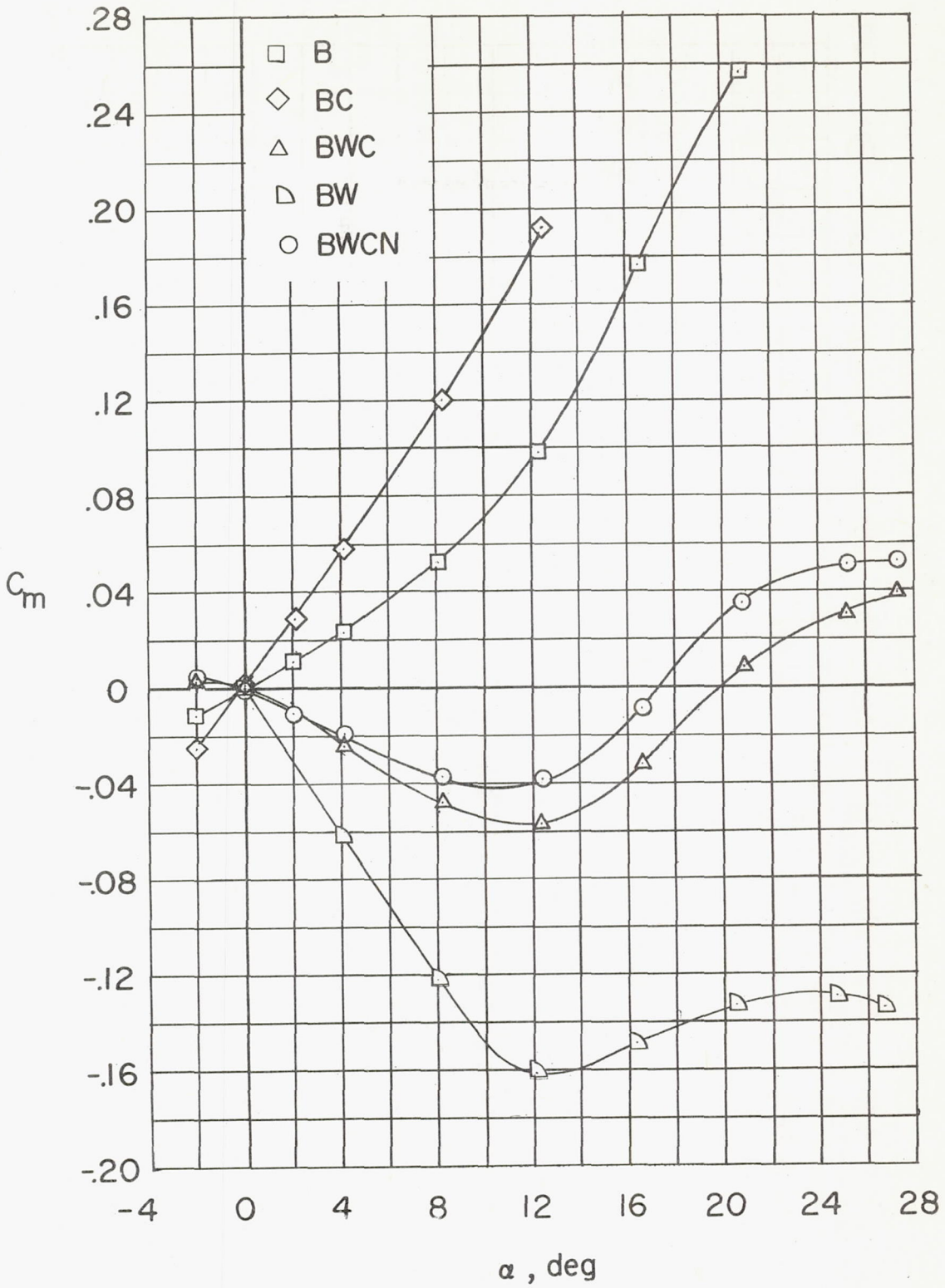


Figure 16.- Aerodynamic characteristics in pitch of the complete model and various combinations of its components; $\beta = 0^{\circ}$.

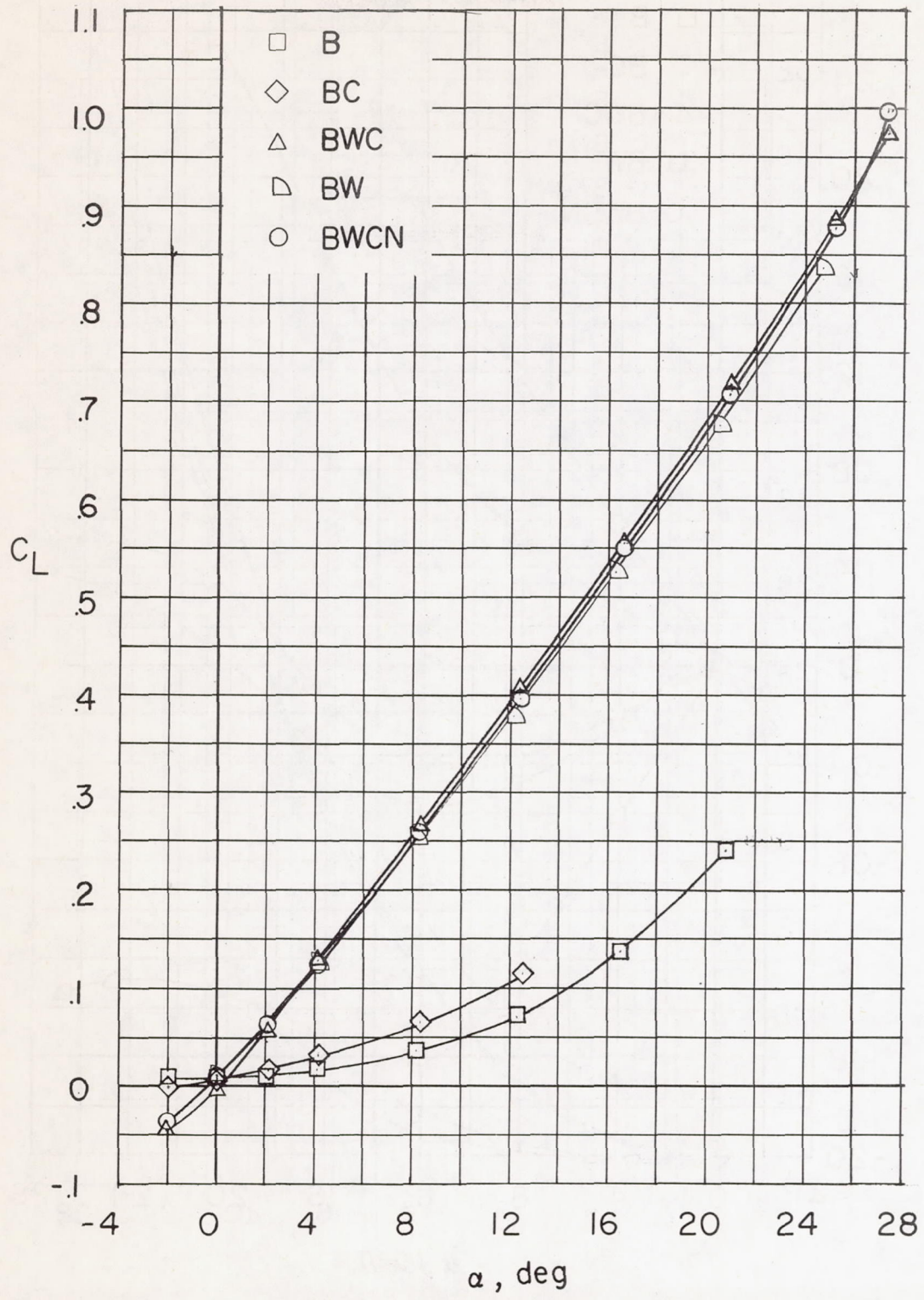


Figure 16.- Continued.

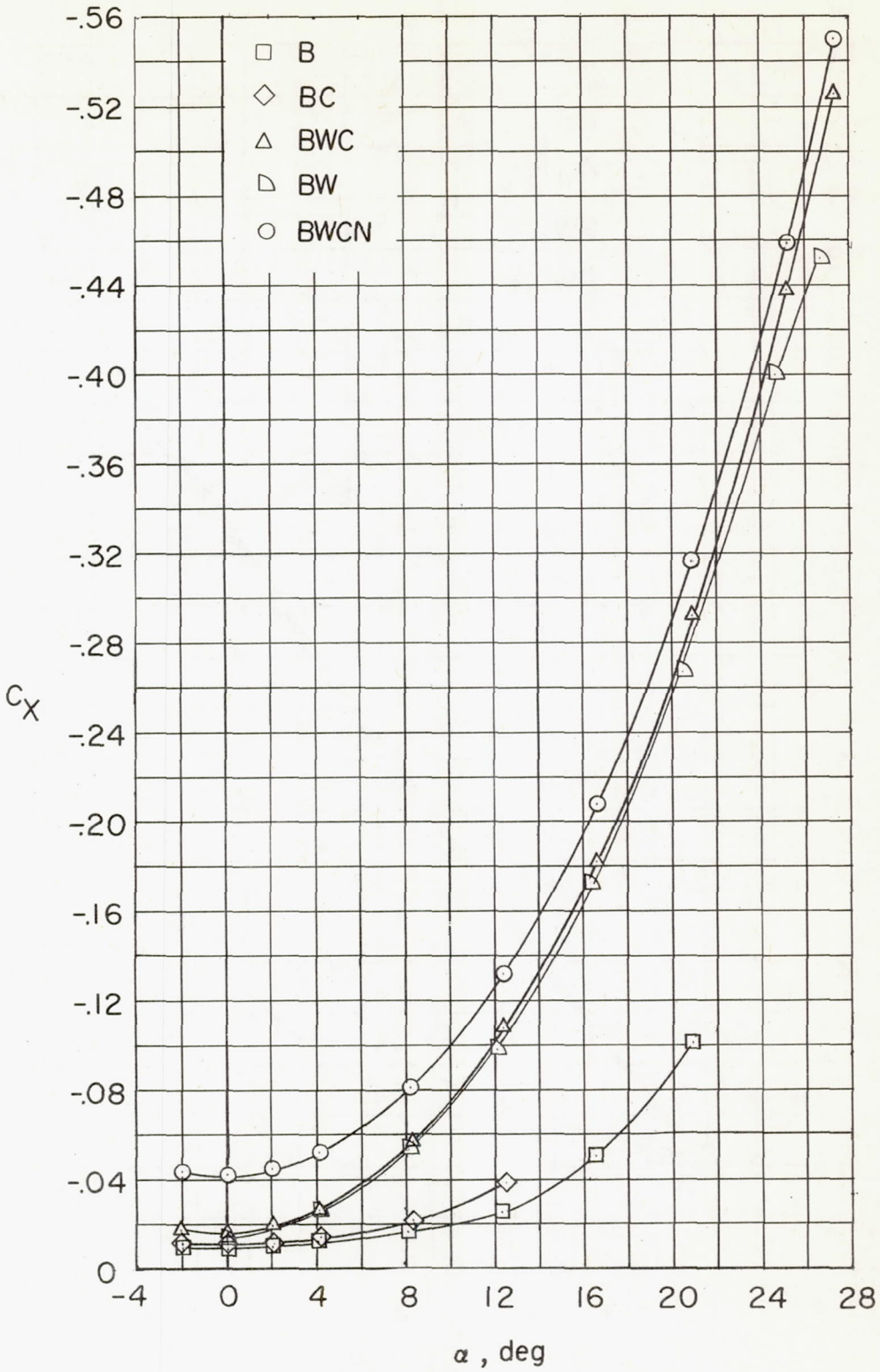


Figure 16.- Concluded.

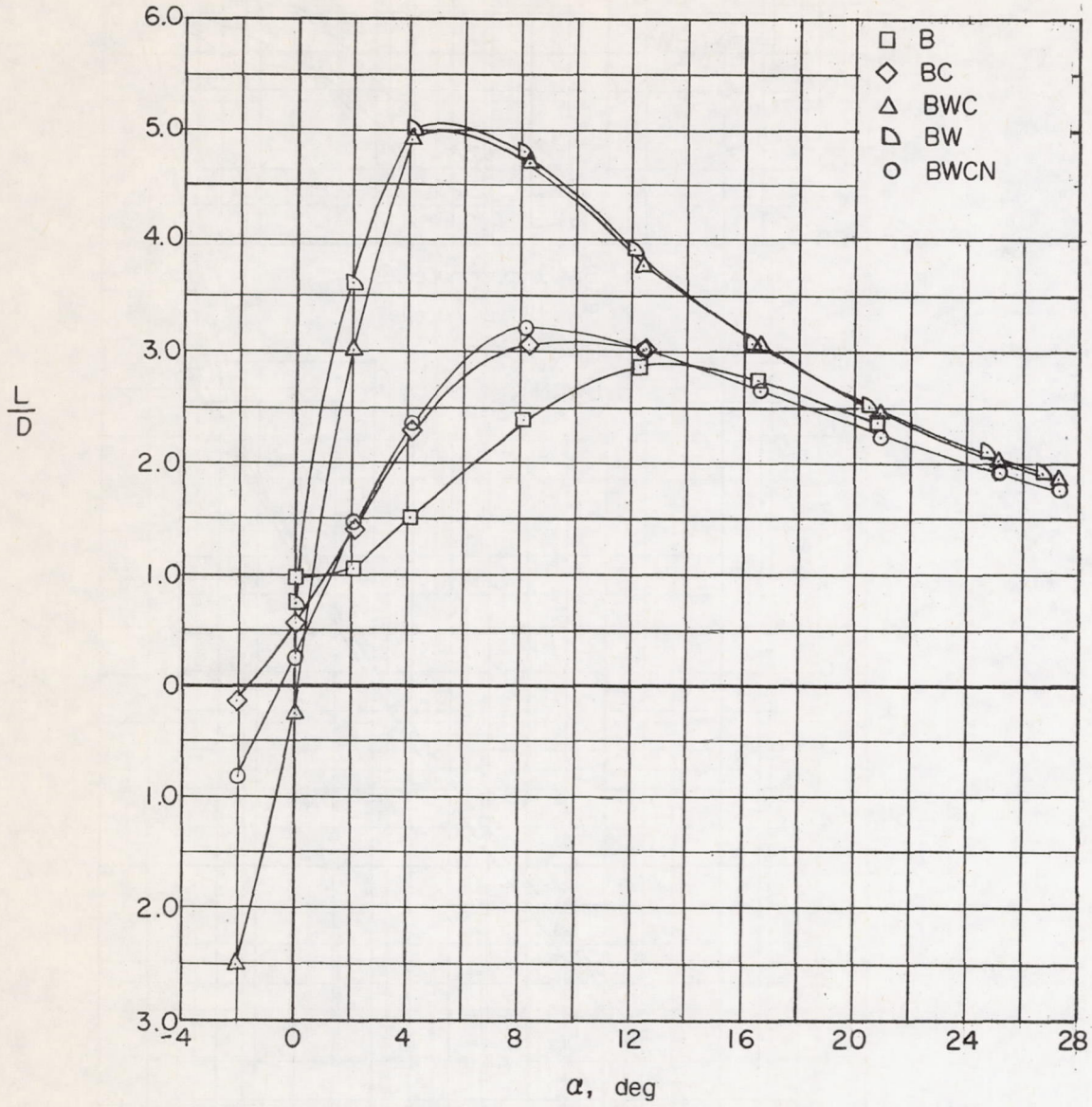


Figure 17.- L/D ratios for the complete model and various combinations of its components; $\beta = 0^{\circ}$.

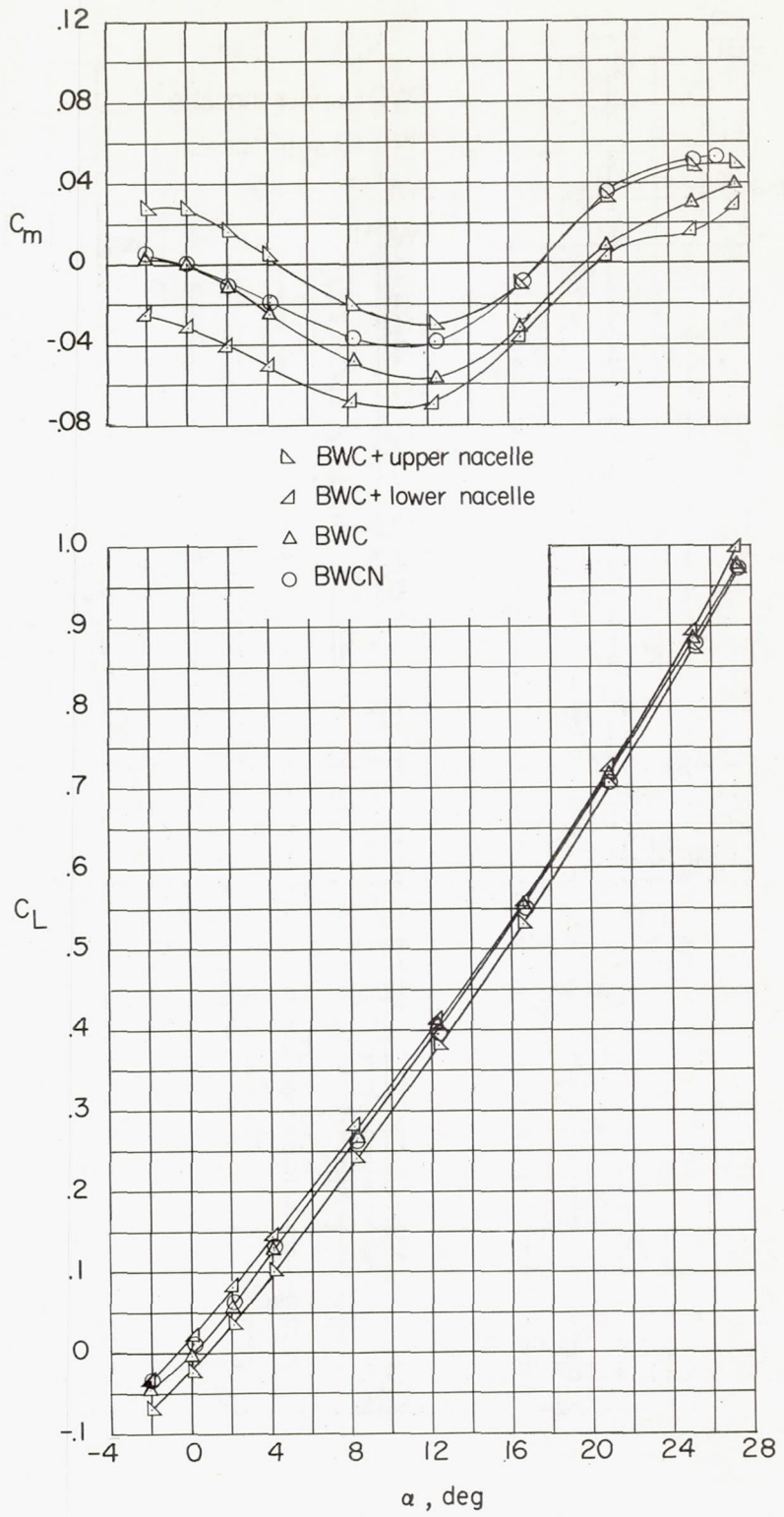


Figure 18.- Effect of nacelle location on the aerodynamic characteristics in pitch; $\beta = 0^{\circ}$.

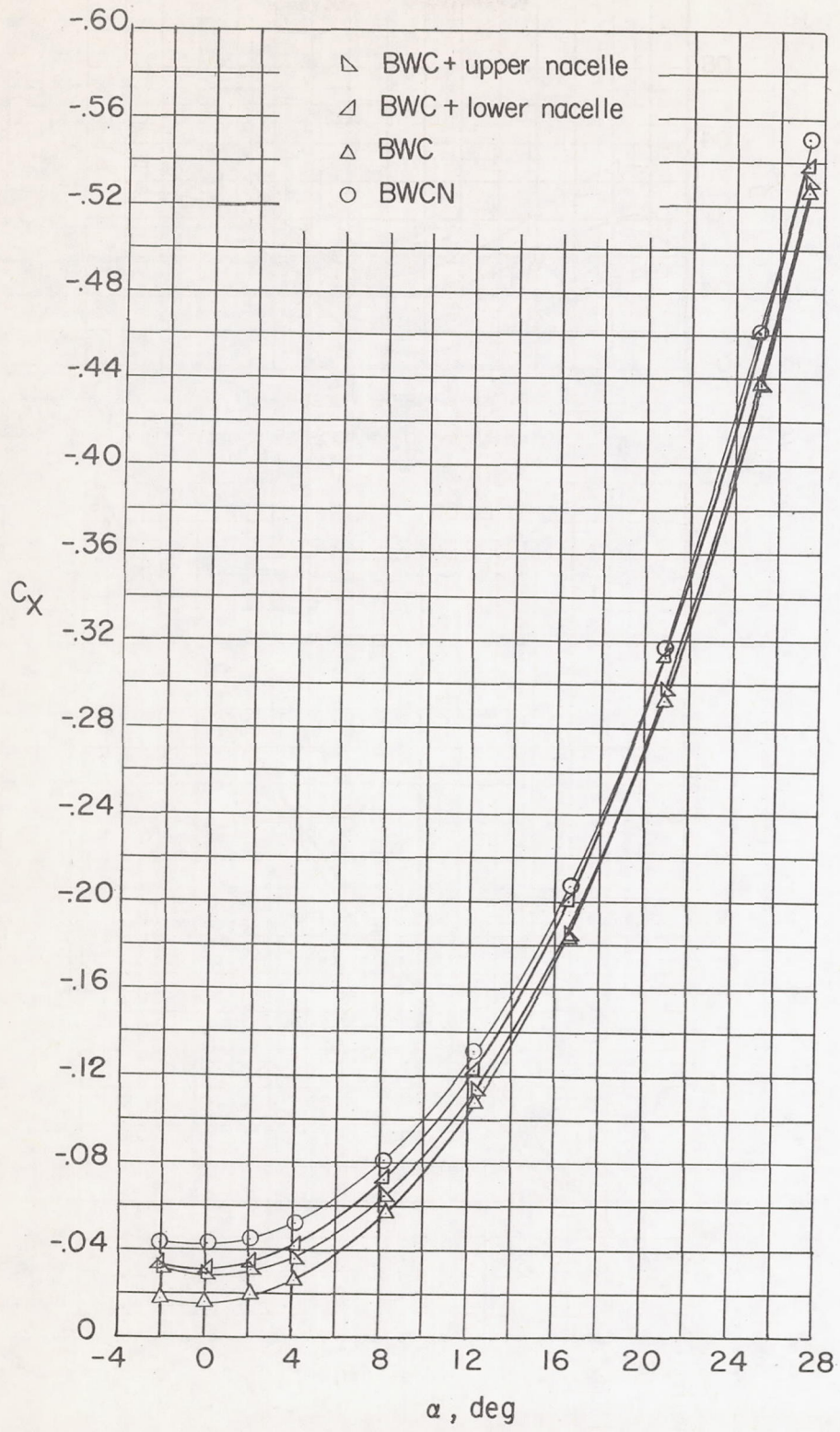


Figure 18.- Concluded.

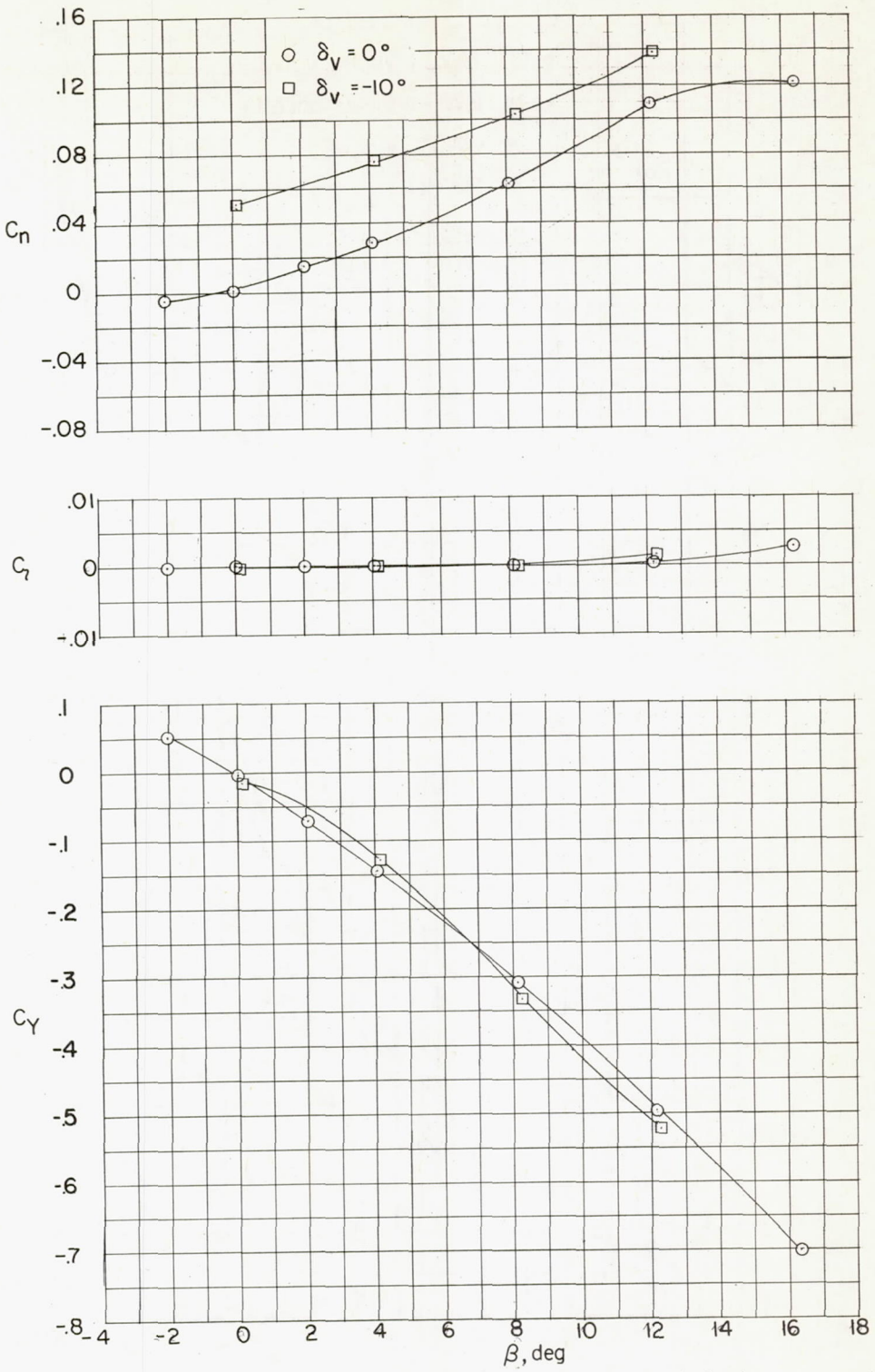


Figure 19.- Aerodynamic characteristics in sideslip at vertical canard deflections of 0^o and -10^o; $\alpha = 0^o$.

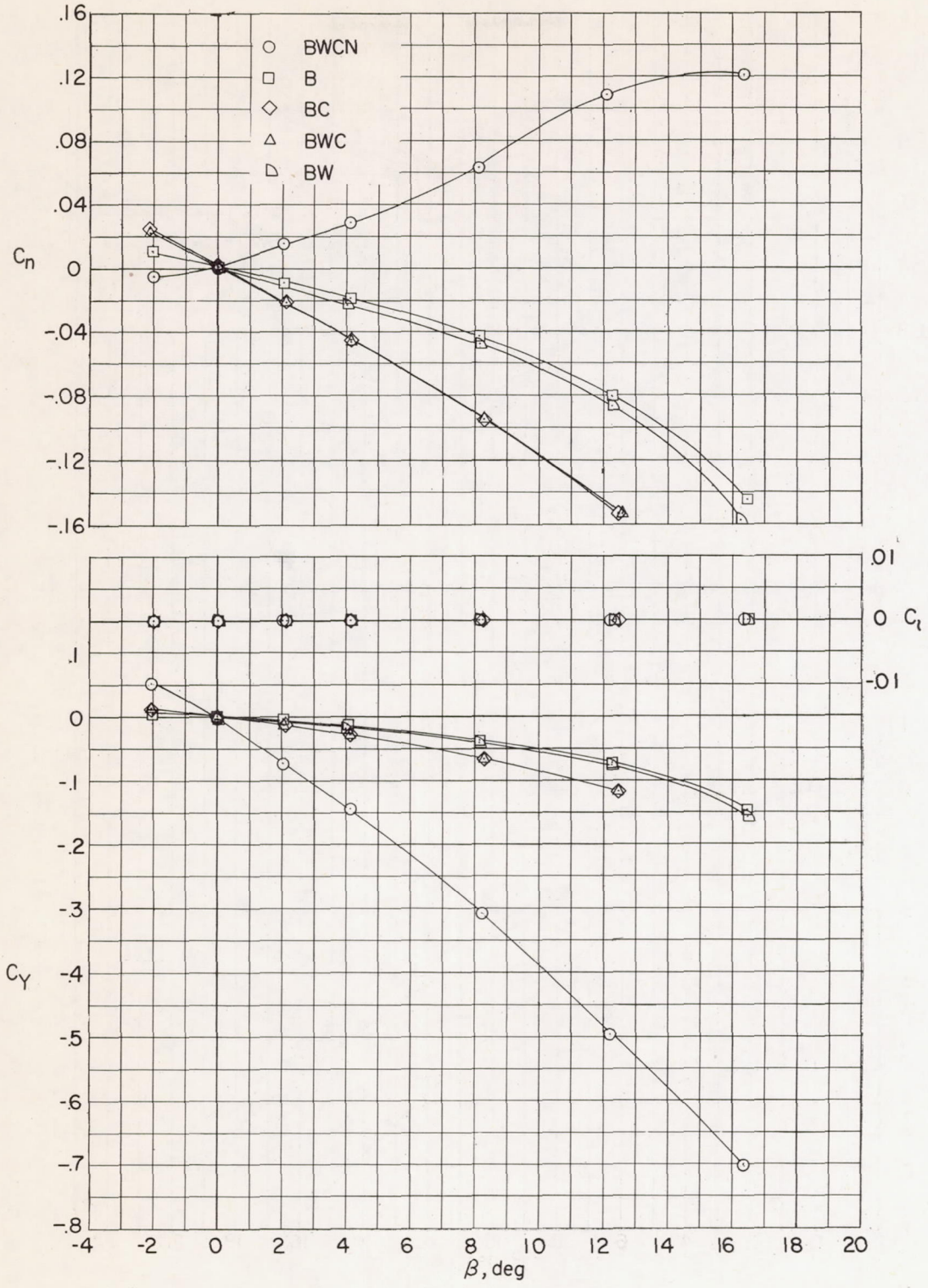


Figure 20.- Aerodynamic characteristics in sideslip for the complete model and various combinations of its components; $\alpha = 0^{\circ}$.

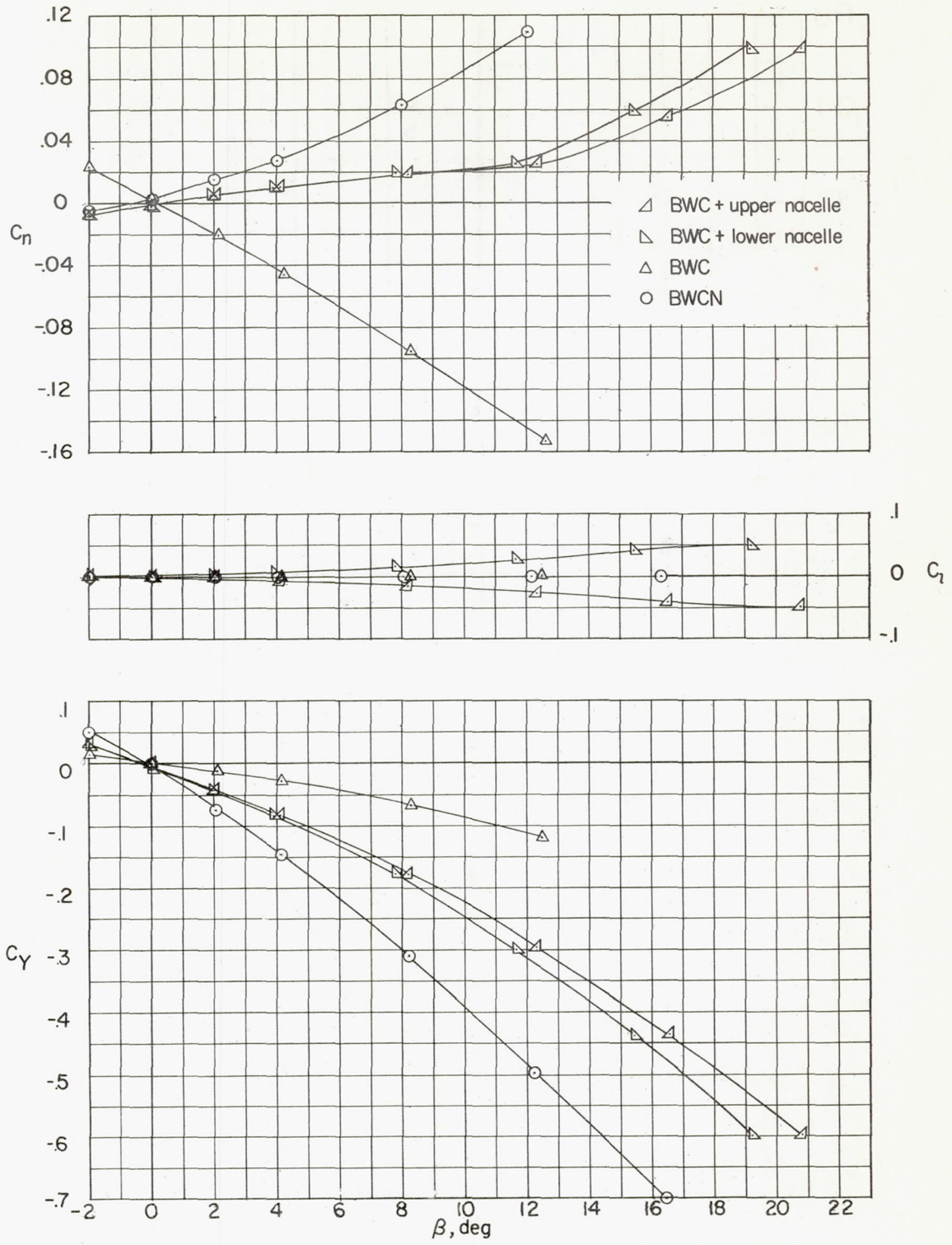


Figure 21.- Effect of nacelle location on the aerodynamic characteristics in sideslip; $\alpha = 0^{\circ}$.

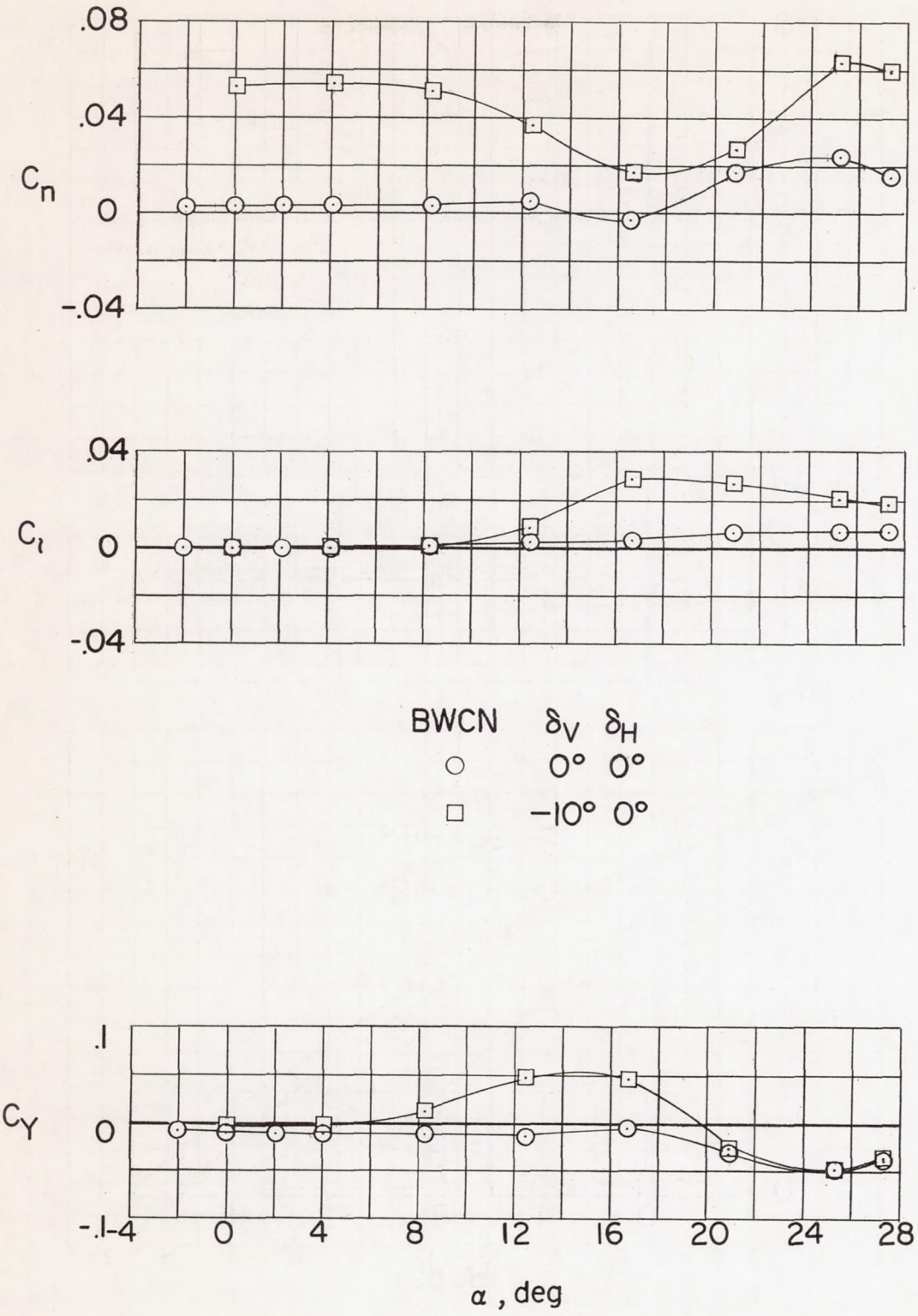


Figure 22.- Effect of vertical canard deflection on the aerodynamic characteristics in pitch; $\beta = 0^\circ$.

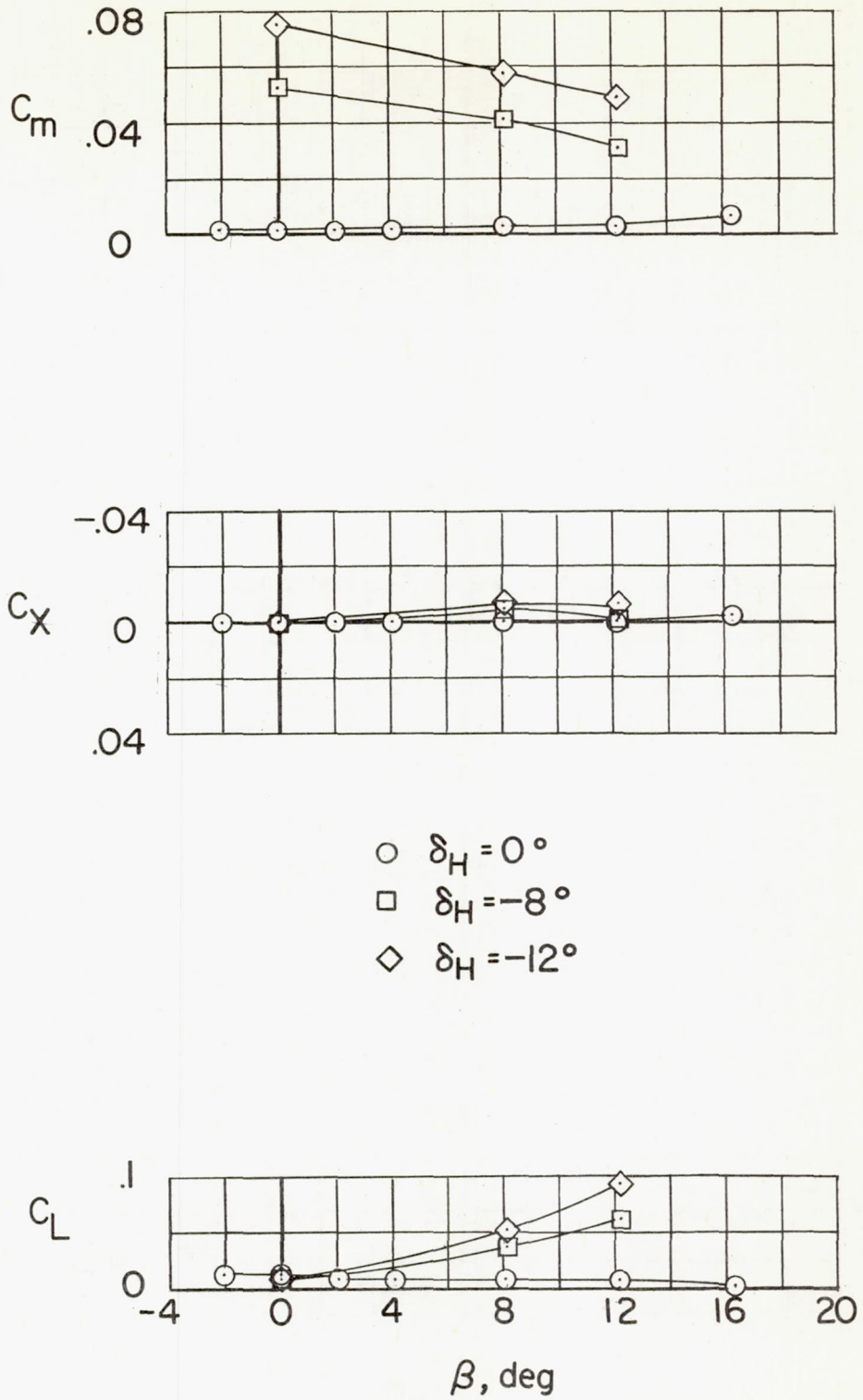


Figure 23.- Effect of horizontal canard deflection on the aerodynamic characteristics in sideslip; $\alpha = 0°$.

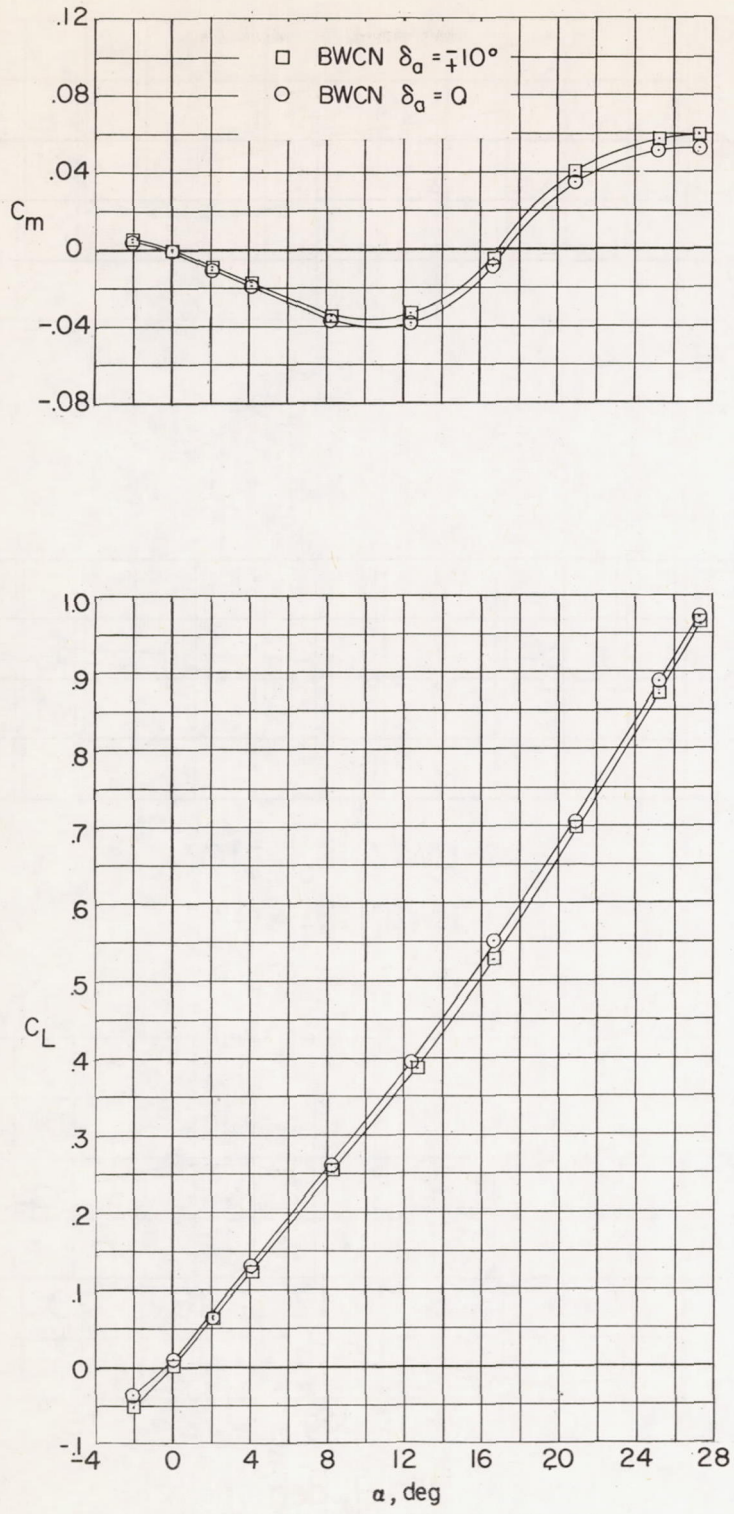


Figure 24.- Effect of aileron deflection on the aerodynamic characteristics in pitch; $\beta = 0^{\circ}$.

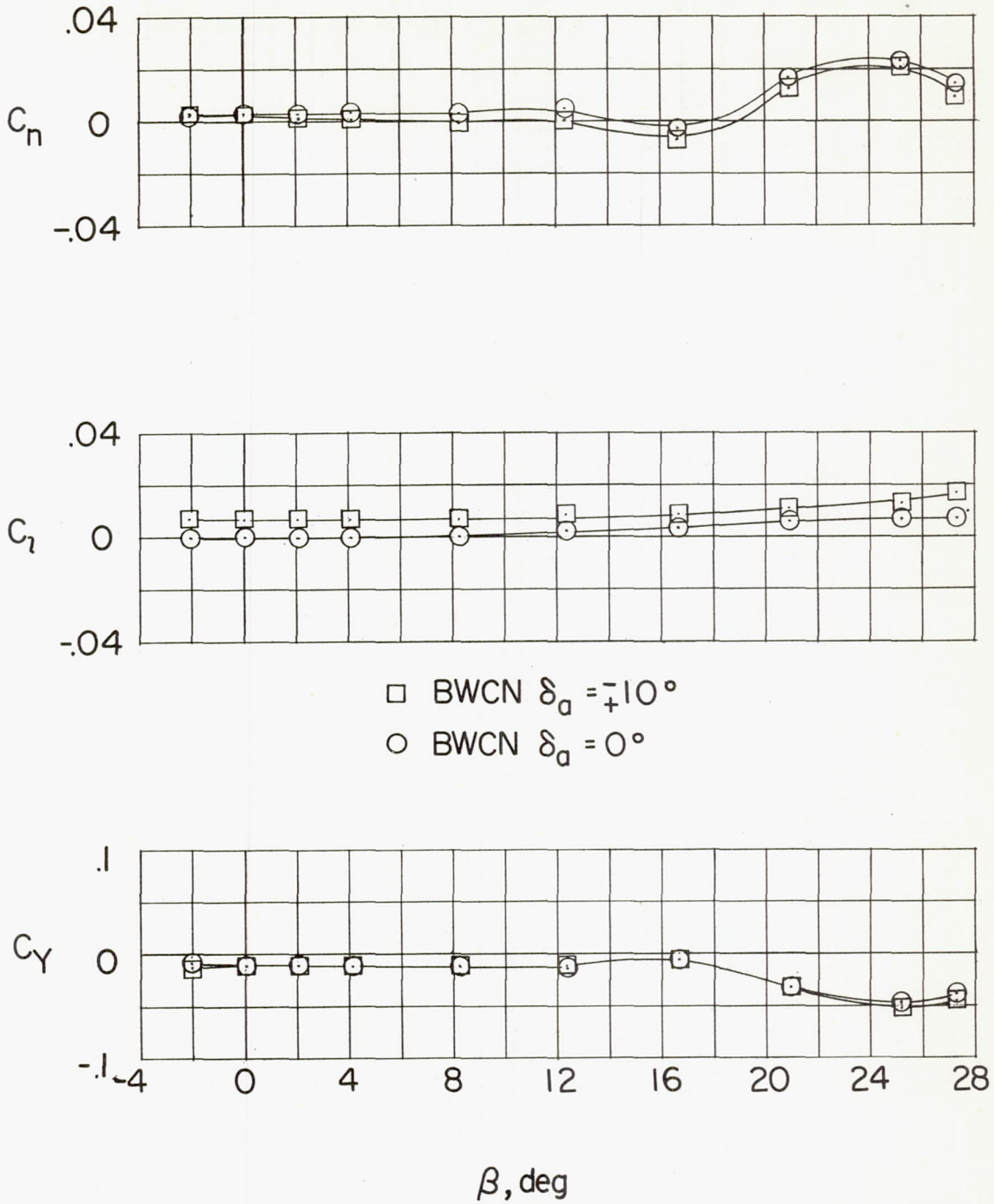


Figure 24.- Continued.

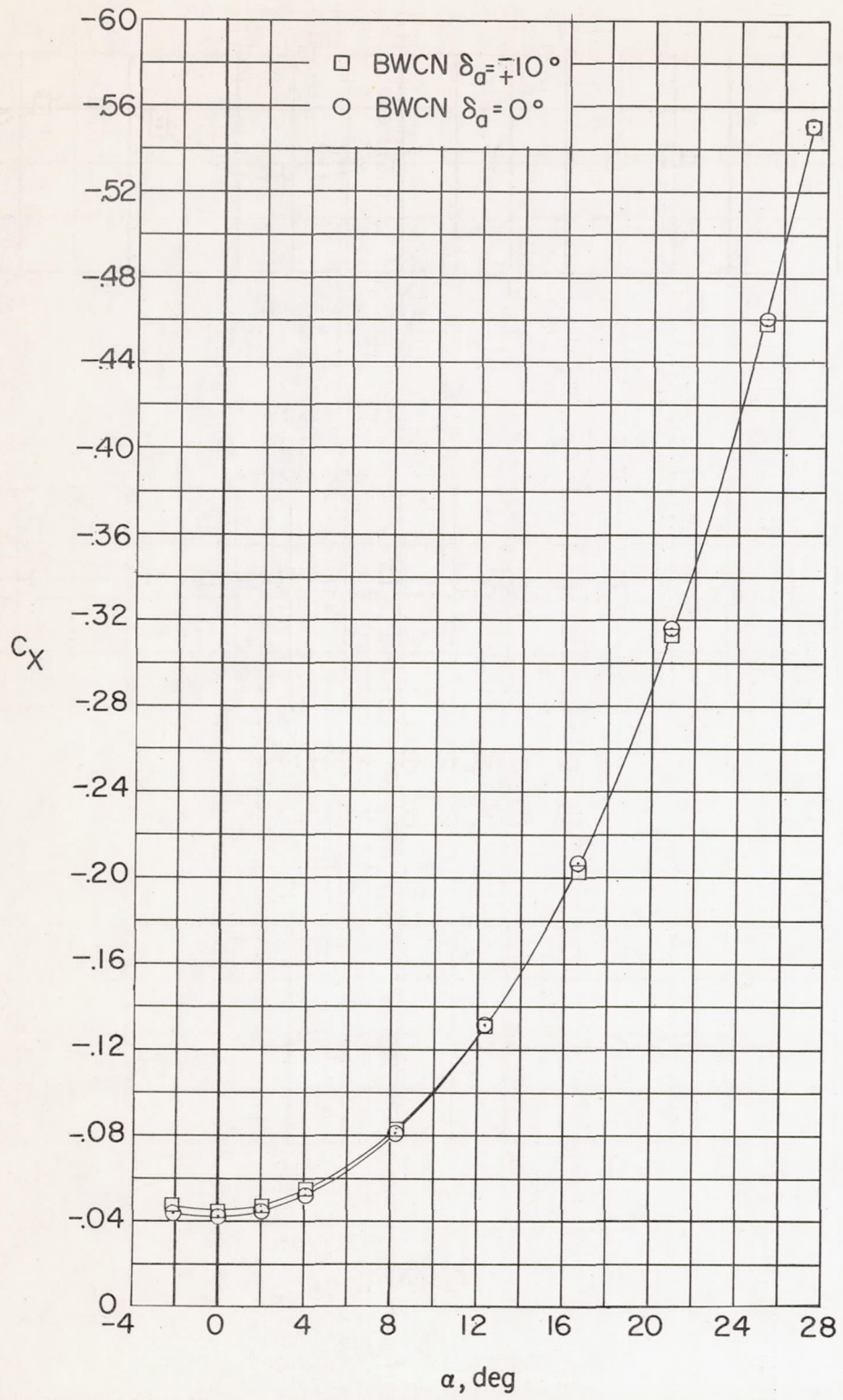
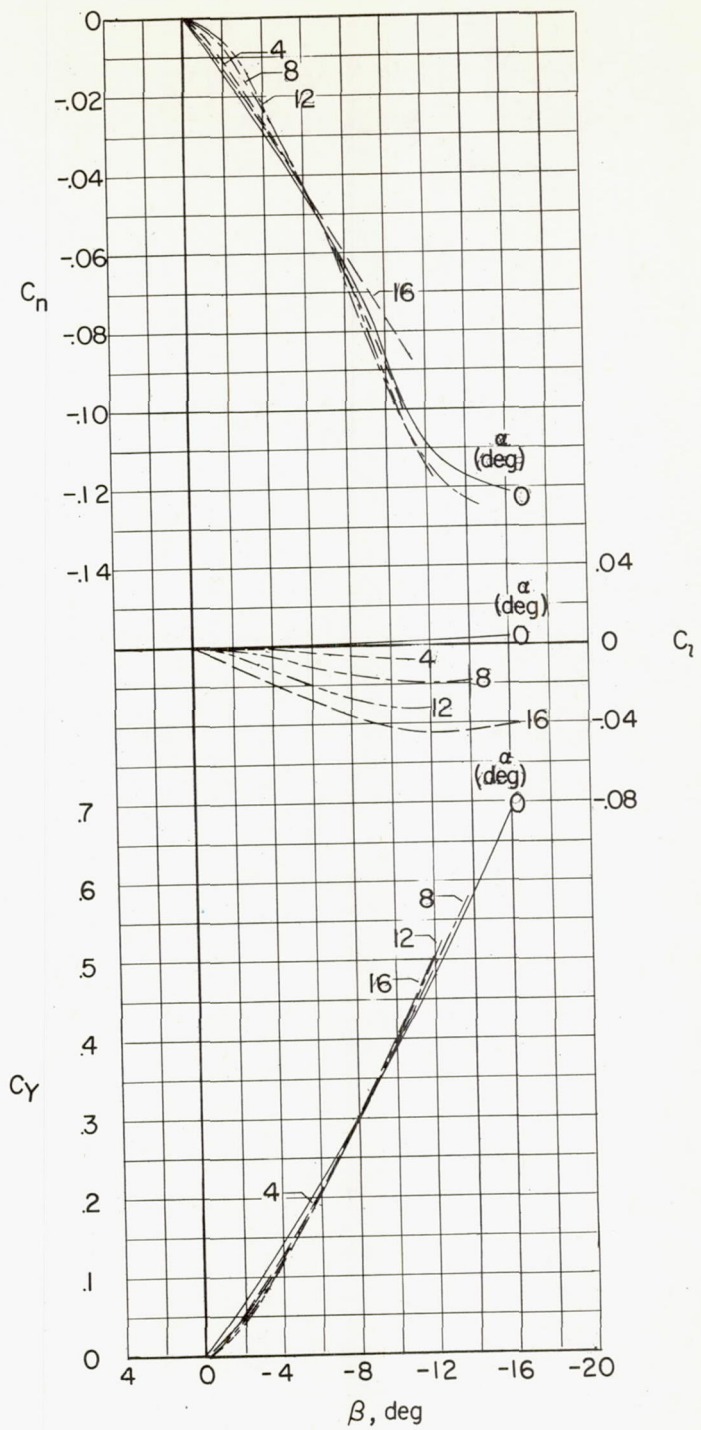
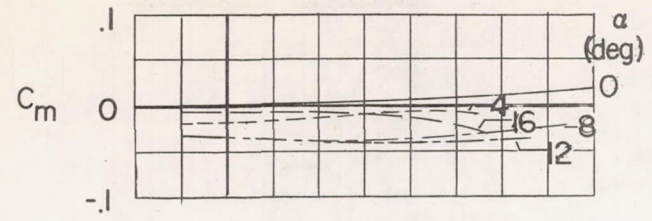


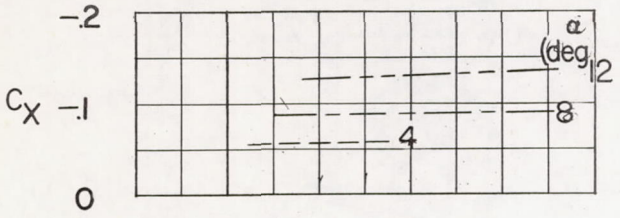
Figure 24.- Concluded.

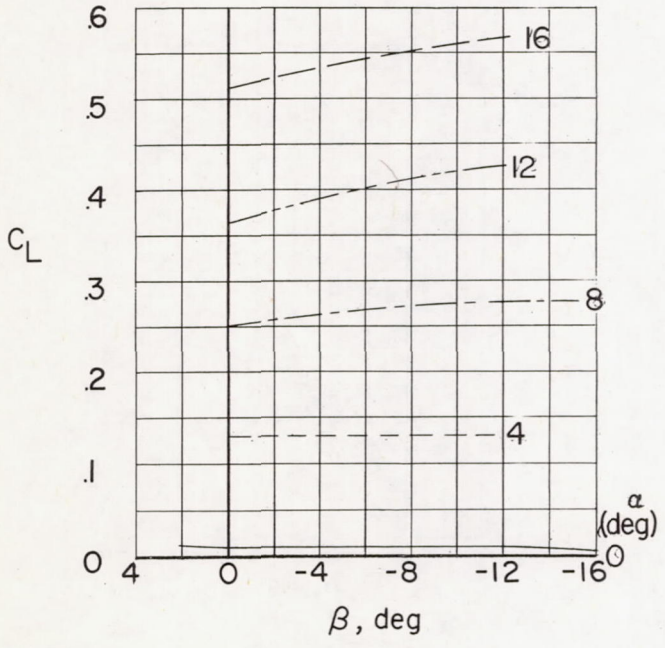


(a) $\delta_H = 0^\circ$; $\delta_V = 0^\circ$.

Figure 25.- Effect of angle of attack on the aerodynamic characteristics in sideslip.

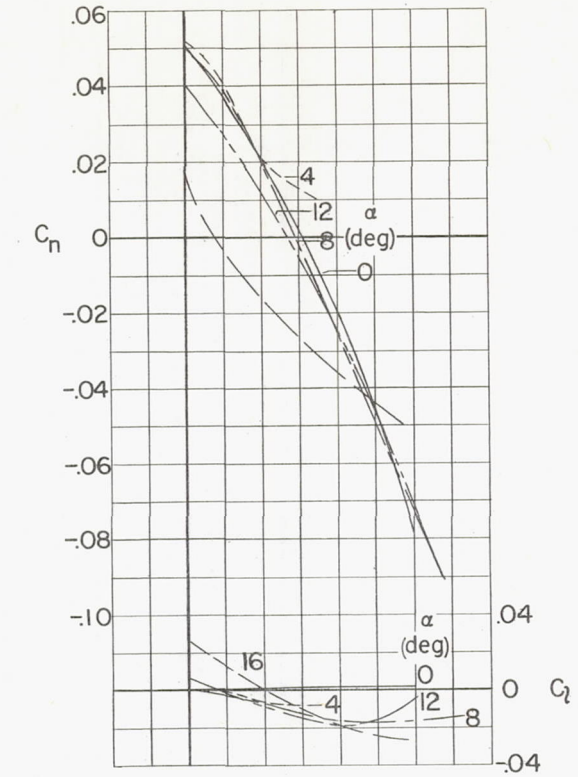


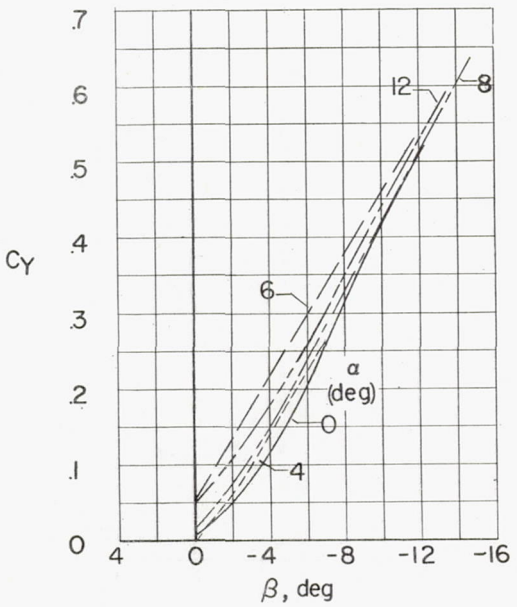




(a) Concluded.

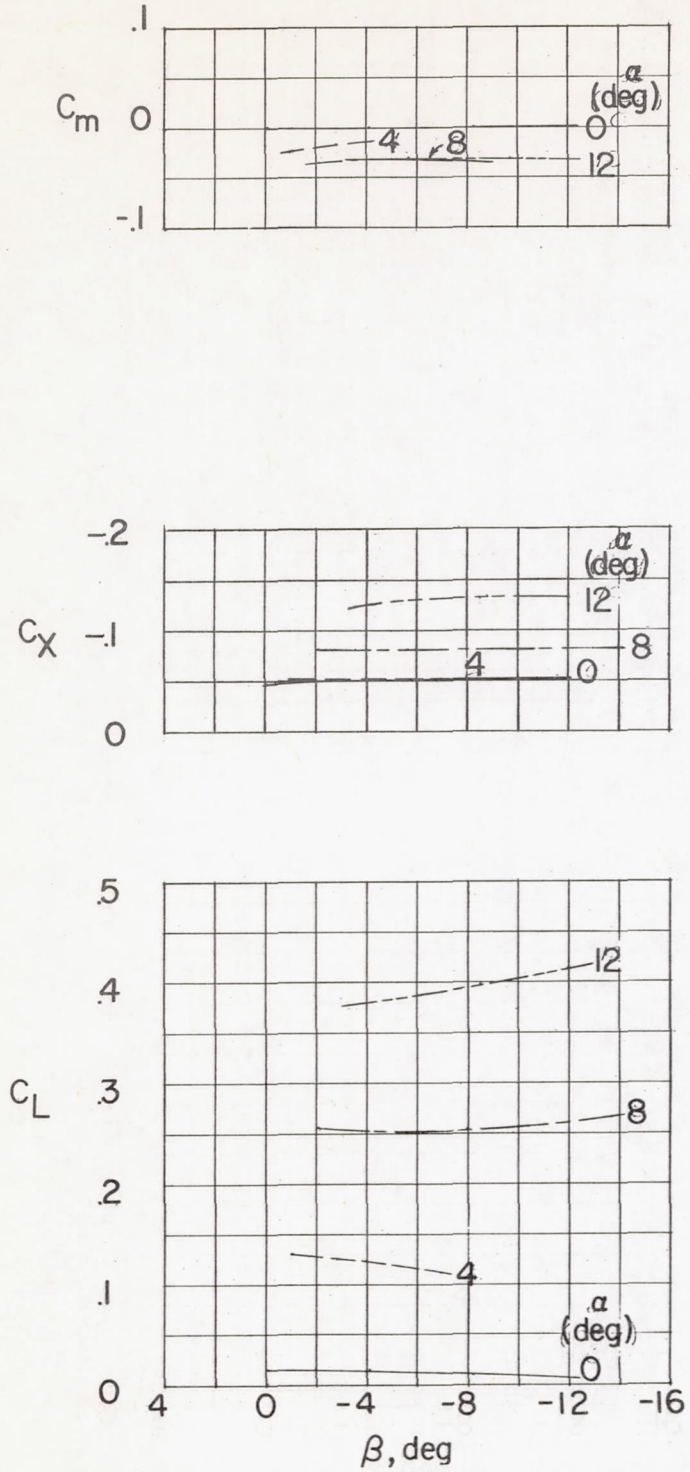
Figure 25.- Continued.





(b) $\delta_H = 0^\circ$; $\delta_V = -10^\circ$.

Figure 25.- Continued.



(b) Concluded.

Figure 25.- Concluded.